Available online at www.sciencedirect.com
SCIENCE DIRECT
Geochimica et Cosmochimica Acta 70 (2006) 164–191
Geochimica
www.elsevier.com/locate/gca

High-precision $^{142}Nd/^{144}Nd$ measurements in terrestrial rocks: Constraints on the early differentiation of the Earth's mantle

Guillaume Caro [a,*], Bernard Bourdon [a], Jean-Louis Birck [a], Stephen Moorbath [b]

[a] *Laboratoire Géochimie-Cosmochimie (UMR 7579 CNRS), Institut de Physique du Globe de Paris, Université Paris 7 Denis Diderot, 4 place Jussieu, 75252 Paris Cedex 05, France*

[b] *Department of Earth Sciences, Oxford University, Parks Road, Oxford OX1 3PR, UK*

Received 29 July 2004; accepted in revised form 25 August 2005

Abstract

We present new ultra-high precision $^{142}Nd/^{144}Nd$ measurements of early Archaean rocks using the new generation thermal ionization mass spectrometer Triton. Repeated measurements of the Ames Nd standard demonstrate that the $^{142}Nd/^{144}Nd$ ratio can be determined with external precision of 2 ppm (2σ), allowing confident resolution of anomalies as small as 5 ppm. A major analytical improvement lies in the elimination of the double normalization procedure required to correct our former measurements from a secondary mass fractionation effect. Our new results indicate that metasediments, metabasalts, and orthogneisses from the 3.6 to 3.8 Ga West Greenland craton display positive ^{142}Nd anomalies ranging from 8 to 15 ppm. Using a simple two-stage model with an initial $\varepsilon^{143}Nd$ value of 1.9 ± 0.6 ε-units, coupled ^{147}Sm–^{143}Nd and ^{146}Sm–^{142}Nd chronometry constrains mantle differentiation to 50–200 Ma after formation of the solar system. This chronological constraint is consistent with differentiation of the Earth's mantle during the late stage of crystallization of a magma ocean. We have developed a two-box model describing ^{142}Nd and ^{143}Nd isotopic evolution of depleted mantle during the subsequent evolution of the crust–mantle system. Our results indicate that early terrestrial protocrust had a lifetime of ca. 0.7–1 Ga in order to produce the observed Nd isotope signature of Archaean rocks. In the context of this two box mantle–crust system, we model the evolution of isotopic and chemical heterogeneity of depleted mantle as a function of the mantle stirring time. Using the dispersion of $^{142}Nd/^{144}Nd$ and $^{143}Nd/^{144}Nd$ ratios observed in early Archaean rocks, we constrain the stirring time of early Earth's mantle to 100–250 Ma, a factor of 5 shorter than the stirring time inferred from modern oceanic basalts.

1. Introduction

Short-lived isotope systems ^{182}Hf–^{182}W and ^{129}I–^{244}Pu–^{129}Xe provide precise chronological constraints on the very early differentiation of the Earth's core (Halliday, 2004; Kleine et al., 2002; Schönberg et al., 2002; Yin et al., 2002) and the formation of terrestrial atmosphere (Kunz et al., 1998; Ozima and Podosek, 1999; Staudacher and Allègre, 1982). In contrast, there are considerable uncertainties about the early history of the Earth's mantle and the nature of the Earth's earliest crust. In particular, the existence of continental crust during the first half billion years of Earth history (e.g., Armstrong, 1968, 1981), and the extent to which terrestrial mantle may have experienced large-scale differentiation following crystallization of a hypothetical magma ocean (e.g., Agee and Walker, 1989; Kato et al., 1988, 1989a,b; Ohtani, 1988), are matters of debate.

With the exception of rare detrital zircons discovered within the Yilgarn craton, Australia (Froude et al., 1983; Compston and Pidgeon, 1986; Wilde et al., 2001), crustal material older than 4.0 Ga is missing from the present-day continental rock record; this precludes direct observation of crust–mantle evolution during the Hadean era (4.0–4.5 Ga). However, insights into early mantle history can be obtained indirectly from the geochemical signatures preserved by isotopic tracers of mantle–crust differentiation.

* Corresponding author. Present address: Division of Geological and Planetary Sciences, California Institute of Technology, Pasadena, CA 91125, USA.
E-mail address: caro@gps.caltech.edu (G. Caro).

0016-7037/$ - see front matter © 2005 Elsevier Inc. All rights reserved.
doi:10.1016/j.gca.2005.08.015

Application of long-lived ^{147}Sm–^{143}Nd isotopic system indicates that early Archaean rocks are characterized by initial $^{143}Nd/^{144}Nd$ ratios higher than chondritic, thereby requiring formation of these rocks from a mantle reservoir with super-chondritic $^{147}Sm/^{144}Nd$ ratio. This, in turn, suggests that the Earth's mantle may have experienced large-scale depletion in incompatible elements several hundred million years prior to the emplacement of the most ancient continental rocks, and more than a billion year prior to the main crustal growth stages (e.g., Chase and Patchett, 1988; Galer and Goldstein, 1991; Smith and Ludden, 1989; Vervoort et al., 1996).

In the framework of the no-continental-growth model, Armstrong (1981) interpreted the depleted Nd signature of early Archaean mantle as a witness of rapid extraction of continental crust prior to 4.0 Ga. However, the lack of a Hadean crustal component in ancient metasediments (Allègre and Rousseau, 1984; Miller et al., 1986; Stevenson and Patchett, 1990) suggests that pre-4.0 Ga continental crust made negligible contribution to early Archaean cratons. This led Chase and Patchett (1988) and Galer and Goldstein (1991) to favor alternative scenarios involving extraction and subsequent recycling of a basaltic rather than a continental protocrust. Unfortunately, models of early mantle–crust evolution largely rely on imprecise estimates of initial $^{143}Nd/^{144}Nd$ ratios of the most ancient early Archaean rocks, whose pristine isotopic signature can be obscured by high-grade metamorphic events (Gruau et al., 1996; Moorbath et al., 1997; Vervoort et al., 1996). Furthermore, a recent examination of ^{176}Lu–^{176}Hf systematics in early Archaean rocks and zircons yielded contrasting results regarding the development of a depleted mantle reservoir early in Earth's history (Bizzarro et al., 2003; Patchett et al., 2004; Scherer et al., 2001; Söderlund et al., 2004). Bizzarro et al. (2003), using a ^{176}Lu decay constant determined on the basis of meteorite age comparison, found that early Archaean rocks and zircons had super-chrondritic initial $^{176}Hf/^{177}Hf$ ratios, in broad agreement with ^{147}Sm–^{143}Nd systematics. However, recent determinations of the ^{176}Lu decay constant by calibration against the U–Pb decay scheme in terrestrial minerals suggest that the decay constant estimated by Bizzarro et al. (2003) may not be applicable to terrestrial samples (Scherer et al., 2001; Söderlund et al., 2004). Using the "terrestrial" ^{176}Lu decay constant would, in turn, imply an early Archaean mantle with near-chondritic $^{176}Lu/^{177}Hf$ ratio. This observation is at odds with the signature of mantle depletion recorded by the ^{147}Sm–^{143}Nd system because Lu/Hf and Sm/Nd fractionation is generally coupled during crustal extraction processes (Vervoort et al., 1999). Therefore, the isotopic record of early Archaean rocks does not provide unambiguous evidence for very early differentiation of the Earth's mantle.

In contrast, short-lived ^{146}Sm–^{142}Nd systematics have the potential to provide precise chronological constraints on very early (>4.2 Ga) mantle differentiation. ^{146}Sm α-decays to ^{142}Nd with a half-life of 103 Ma. Given the sensitivity in modern isotope measurement techniques, $^{142}Nd/^{144}Nd$ variations are undetectable if Sm/Nd fractionation occurred after 4.2 Ga, and hence ^{142}Nd is specifically sensitive to the earliest mantle differentiation processes. In addition, the negligible abundance of ^{146}Sm after 4.0 Ga makes the $^{142}Nd/^{144}Nd$ ratio of early Archaean rocks less sensitive to metamorphic disturbance than their $^{143}Nd/^{144}Nd$ ratio.

The presence of extinct ^{146}Sm in the early solar system was first demonstrated by Lugmair and Marti (1977), who determined an initial $^{146}Sm/^{144}Sm$ ratio of 0.0047 ± 23 at 4.56 Ga from mineral separates of the meteorite Angra Dos Reis (ADOR). However, subsequent attempts to estimate the initial $^{146}Sm/^{144}Sm$ using mineral isochrons on meteorites yielded conflicting results, ranging from ca. 0.0045 (Lugmair et al., 1983; Nyquist et al., 1990) to 0.012 (Jacobsen and Wasserburg, 1984). Higher values ($\approx$0.015) were reported by Prinzhofer et al. (1989) but these were interpreted as reflecting partial re-equilibration of the ^{147}Sm–^{143}Nd system during late (>4.0 Ga) metamorphism, resulting in age uncertainties and spurious estimates of the initial $^{146}Sm/^{144}Sm$ ratio (Prinzhofer et al., 1992). These mixed results were subsequently discussed by Lugmair and Galer (1992) who also report an initial $^{146}Sm/^{144}Sm$ ratio of 0.0071 ± 17 for ADOR. These authors combined all the literature data and estimated an initial $^{146}Sm/^{144}Sm$ ratio of 0.007 ± 1 at the time of formation of the solar system (4.56 Ga). This value is in agreement within errors with the value of 0.008 ± 1 previously suggested by Prinzhofer et al. (1992) and with more recent estimates (Amelin and Rotenberg, 2004; Nyquist et al., 1994). In what follows, we will adopt a mean $^{146}Sm/^{144}Sm$ value of 0.008 ± 1. The model age calculations presented in this study are not significantly affected by the aforementioned uncertainty on the initial $^{146}Sm/^{144}Sm$ ratio.

^{142}Nd anomalies in early Archaean mantle are not expected to exceed 30 ppm due to the extremely low initial abundance of ^{146}Sm in the solar system and the small $\varepsilon^{143}Nd$ values (+1 to +3 ε-units) observed in early Archaean rocks. Consequently, their detection is analytically challenging and previous attempts to measure $^{142}Nd/^{144}Nd$ in early Archaean rocks yielded inconsistent and highly controversial results. Harper and Jacobsen (1992), and Goldstein and Galer (1992) first attempted to apply ^{146}Sm–^{142}Nd chronometry to early Earth differentiation. Harper and Jacobsen (1992) reported 6 analyses of a 3.7–3.8 Ga Isua metasediment (IE 71528) showing a $^{142}Nd/^{144}Nd$ excess of 33 ppm (with external precision of 10 ppm (2σ)). However, Goldstein and Galer (1992) and subsequent studies (McCulloch and Bennett, 1993; Regelous and Collerson, 1996) failed to detect ^{142}Nd anomalies in Archaean samples from West Greenland, Australia, South Africa, and North Canada. This led Sharma et al. (1996) to investigate all potential sources of uncertainty in high-precision $^{142}Nd/^{144}Nd$ measurements by thermal-ionization mass spectrometry (TIMS). After a series of experiments, Sharma et al. (1996) concluded that they were unable to reproduce

^{142}Nd data to the level of precision reported by Harper and Jacobsen (1992) but found strong hints of a 30 ± 20 ppm (2σ, $N = 10$) anomaly in two metasediments from Isua, including the sample analyzed by Harper and Jacobsen (1992). However, these authors reported a strong dependence of measured Nd isotope ratios on focusing settings of the MAT262 mass spectrometer, with a magnitude as high as 40–60 ppm on the ^{142}Nd/^{144}Nd ratio. More recently, Boyet et al. (2003) measured ^{142}Nd/^{144}Nd by MC-ICPMS in metabasalts and metagabbros from the western Isua belt and found that 3 out of 8 samples had positive ^{142}Nd anomalies of 30 ± 20 ppm (2σ). However, our examination of the ^{146}Sm–^{142}Nd systematics of early Archaean rocks using more precise mass spectrometric techniques yielded rather different results. In a previous contribution, we reported measurements of the ^{142}Nd/^{144}Nd ratios in early Archaean metasediments from Isua (West Greenland, 3.7–3.8 Ga) using the Thermo Electron Triton, a new generation of thermal-ionization mass spectrometers (Caro et al., 2003a). Our first results showed that the ^{142}Nd/^{144}Nd ratio could be determined with long-term external precision of 5 ppm (2σ; $N = 33$), a factor of 3 below reproducibility reported in previous studies. We reported 23 analyses of 7 mafic metasediments from the northeastern part of the Isua greenstone belt yielding indistinguishable ^{142}Nd anomalies of 15 ± 4 ppm (2σ). The small magnitude of these anomalies makes them undetectable at the level of precision reported in previous studies (Goldstein and Galer, 1992; Harper and Jacobsen, 1992; McCulloch and Bennett, 1993; Regelous and Collerson, 1996; Sharma et al., 1996). Likewise, Sharma and Chen (2004) re-analyzed two aliquots of sample IE 715-28 using more precise analytical techniques but found no resolvable anomaly at the 2σ level of precision, both aliquots yielding $100 \times \varepsilon^{142}\text{Nd} = 5 \pm 8$ ppm ($2\sigma_m$). These new high-precision results cast some doubts on the existence of large ^{142}Nd anomalies (>20 ppm) in Isua rocks and clearly suggest that application of ^{146}Sm–^{142}Nd systematics to early Earth differentiation requires determination of Nd isotope ratios to better than 5 ppm (2σ).

Here, we present new high-precision data for a wide range of early Archaean rocks from Acasta (4.0 Ga), the Godthaabsfjord and Isua regions (3.65–3.8 Ga), and Barberton (3.5 Ga) using further improved measurement techniques allowing the determination of ^{142}Nd/^{144}Nd ratios with an external precision of 2 ppm (2σ; $N = 30$). We report systematic deviations of 7.6 ± 2.7 ppm ($2\sigma_m$) to 15.4 ± 2.3 ppm ($2\sigma_m$) in all lithologies from the early Archaean Greenland craton. In contrast, no anomaly could be detected in samples from Acasta and Barberton. Our results contrast with those obtained by Harper and Jacobsen (1992) and Boyet et al. (2003) who report anomalies as high as 30 ppm in Isua rocks and strongly argue against significant heterogeneities of ^{142}Nd/^{144}Nd ratios within Isua metabasalts as advocated by Boyet et al. (2003). Rather, ^{142}Nd anomalies in the 3.7–3.8 Ga Isua belt and adjacent gneisses seem ubiquitous and, although ^{142}Nd signatures may vary slightly between different lithologies around a mean value of 10 ppm, samples from a given geological unit display only minor heterogeneity.

2. Regional geology and sampling strategy

2.1. Southern West Greenland

All samples were collect by S. Moorbath (see Fig. 1 for sample location). They represent a range of rock types from the complex early Archaean (ca. 3.65–3.82 Ga) terrane of southern West Greenland, which has been described by many workers for some thirty years. Here, we discuss salient features of the individual rock associations studied in the present work, all of which exhibit positive ε^{142}Nd anomalies.

2.1.1. Metamorphosed clastic sediments from the Isua greenstone belt

This group comprises samples 248443, 248484A, 93/13, 93/33, 93/57, 97/31, and 99/15 (the common prefix SM/GR/for the last five samples is omitted in the text). They come from the eastern sector of the ca. 3.7–3.8 Ga Isua greenstone belt (IGB), within a ca. 3 km radius of the Isua base camp (led by P.W.U. Appel) at N65°10.198, W49°48.808.

Recent accounts of the metamorphic evolution and mineralogy of the IGB have been given by Hayashi et al. (2000) and Rollinson (2002). Detailed major, minor, and trace element (including REE) analyses on IGB clastic metasediments are given in Bolhar et al. (2005).

The first six samples listed above are identified as mafic-to-intermediate, pelitic sediments (“metapelites”). It is emphasized that their mineralogy is entirely metamorphic and, therefore, secondary in origin. They consist of variably deformed, banded garnet–biotite–plagioclase (±hornblende, quartz, muscovite, staurolite, epidote, zoisite, and tourmaline) schists. Zircons appear as rare, tiny grains. Field collecting steered clear of any obvious metasomatic infiltrations (which are, in any case, not common in these rocks), but in thin section some samples show minor secondary patches and veinlets of calcite and quartz.

Twenty-four IGB metapelite samples, including several of the above, have yielded a Sm–Nd whole rock regression age of 3744 ± 46 Ma, with an initial ε^{143}Nd of $+1.9 \pm 0.6$ ε-units, regarded as minimum age of sediment deposition (Kamber et al., 1998). Five of the present samples (93/13, 93/33, 93/57, 248443, 248484A) were already shown to contain ^{142}Nd anomalies in previous work (Caro et al., 2003a), and they have been re-analyzed here using more precise analytical techniques.

Sample 99/15 is from a prominent horizon of felsic volcanogenic sediments in the eastern sector of the IGB (N65°10.187, W49°50.353). These fine-grained banded rocks contain plagioclase, quartz, K-feldspar, muscovite, biotite, epidote, and accessory minerals (SiO_2 ca. 70%). A zircon U–Pb date of 3710 Ma has been reported by Nutman et al. (1997) on the same unit. Sample 99/15 was

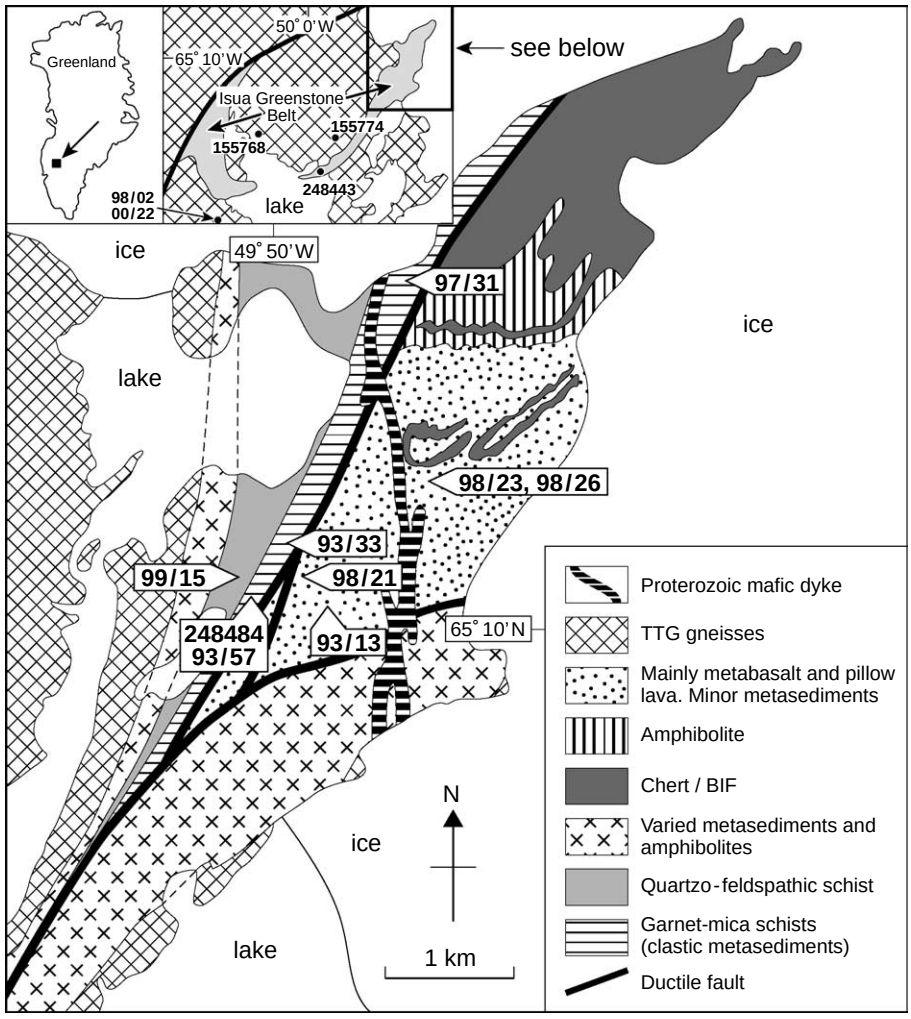

Fig. 1. Geological sketch map of the easternmost sector of the Isua greenstone belt (IGB), southern West Greenland, showing sample localities. Note position of IGB in Greenland (left inset) and position of easternmost sector relative to the entire IGB (right inset). Some of the more distant sample localities are shown in the right inset. For the sake of clarity, the prefix SM/GR/ is omitted where appropriate. Two of the analyzed samples (155702, 155706) are not shown. They are from the type area of Amitsoq gneiss in the outer Godthaabsfjord region, some 150 km southwest of the IGB (see Fig. 2 from Moorbath et al., 1972).

collected close to a sharp contact with typical garnet–mica schists as described above, and specifically ≈80–100 m from the closely spaced samples 248484A and 93/57 (see above).

The whole-rock regression explanation contrasts with that of Jacobsen and Dymek (1988), who studied ^{147}Sm–^{143}Nd (and ^{87}Rb–^{87}Sr) isotope systematics of the IGB metasediments and other rocks. Their point-by-point interpretation of the isotopic data led them to postulate a significant range in initial $\varepsilon^{143}Nd$ values, suggesting widely heterogeneous mantle sources as well as a large volume of pre-3.8 Ga crust. Gruau et al. (1996) and Moorbath et al. (1997), however, regarded this apparent range of initial $\varepsilon^{143}Nd$ values as the result of statistical geological scatter induced by one or more post-depositional, tectonothermal disturbances, which are well documented in the region. We therefore regard the ^{147}Sm–^{143}Nd regression (errorchron) data of Kamber et al. (1998) on the metasediments (see Section 2.1.1) as a better estimate of their true age and initial ratio.

2.1.2. Metamorphosed basaltic rocks from the Isua greenstone belt

This group comprises samples 98/21, 98/23, and 98/26, also from the eastern IGB. They come from two closely studied localities of metabasaltic rocks of exceptionally low strain (Appel et al., 1998) within the generally highly deformed rocks of the IGB. All three samples are from structurally well-preserved pillow lavas, but with entirely metamorphic (secondary) mineralogy. Sample 98/21 is a pillow basalt from the first locality of convincing pillow lavas discovered in the IGB in 1991 (N65°10.377, W49°49.353). Sample 98/26 is a pillow basalt from a locality discovered in 1998 by M. Solvang (N65°10.838, W49°48.288). Sample 98/23 consists of a microcrystalline pillow rim from this locality. A brief discussion of the

reported ^{147}Sm–^{143}Nd systematics on metabasalts (Polat et al., 2003) is given in Section 3.1.

It may be noted that the above samples are from a different region of the IGB than the metabasaltic samples measured by Boyet et al. (2003), who report that three of their samples, out of eight analyzed, carried a ^{142}Nd excess of 30 ± 20 ppm, whilst the remaining samples had no measurable ^{142}Nd excess.

2.1.3. Gneisses of magmatic origin (orthogneisses)

This group comprises samples 155702, 155706, 155768, and 155774, and SM/GR/98/2. They represent three of the main regions of early Archaean granitoid (TTG-type) orthogneisses in southern West Greenland.

Samples 155702 and 155706 are from the Godthaabsfjord region, near Narssaq. Sample localities and descriptions are given in Fig. 1 and Moorbath et al. (1972), where a whole-rock Rb–Sr regression age of 3.66 Ga (revised with modern decay constant) was reported for these and other samples. A detailed review of published age work on these Itsaq (formerly Amîtsoq) gneisses is given in Kamber et al. (2001), where a regional emplacement age of ca. 3.65 Ga is favored for the magmatic precursor of the orthogneisses. These authors also discussed a combined ^{147}Sm–^{143}Nd regression (errorchron) age of 3640 ± 120 Ma with an initial $\varepsilon^{143}Nd = 0.9 \pm 1.4$ for a large array of Itsaq gneisses. Scatter in excess of analytical error about the regression line may result either from open-system behavior during much later metamorphism, or to a small degree of heterogeneity in initial Nd isotope ratios for different Itsaq gneiss components, or to both. Nevertheless, the ^{147}Sm–^{143}Nd regression parameters (as well as numerous concordant whole-rock Rb–Sr, Pb/Pb, and zircon U–Pb dates) are regarded as a close approximation to the age and initial ratios of the bulk of the Itsaq gneisses.

Samples 155768 and 155774 are typical orthogneisses from the Isua area, ≈150 km northeast of the Godthaabsfjord gneisses. Here, the IGB forms a semicircle, some 25 km in diameter, of steeply dipping schists around a core of tonalitic to granitic rocks. The two samples used here form part of the original age study of Moorbath et al. (1972), with a reported whole-rock Rb–Sr age of ca. 3.61 Ga. The most recent age study of the Isua region gneisses, which also summarizes previous age work, is by Crowley et al. (2002), who provide U–Pb ages ranging from 3.6 to 3.7 Ga.

Sample 98/2 (N65°02.70, W50°08.36) is a fine-grained, weakly banded, gray plagioclase–quartz–biotite–hornblende gneiss from an extensive region of tonalitic-to-granitic orthogneisses immediately to the south of the IGB, which could be the oldest well-preserved granitoid rock on Earth. The oldest zircon U–Pb dates on these gneisses are in the range 3.81–3.82 Ga (Crowley, 2003; Nutman et al., 1999). An ion-probe U–Pb date on zircon from sample 98/2 itself gave an age of 3812 ± 14 Ma (Kamber et al., 2003).

2.1.4. Enclave in 3.82 Ga gneisses

The 3.82 Ga orthogneisses south of the Isua region (see above) host numerous older enclaves of diverse sizes and compositions (Friend et al., 2002). Sample 00/22 (N65°01.532, W50°13.343) are from a medium-grained, banded amphibolite enclave, composed of hornblende, plagioclase, and minor sphene. Its minimum age is defined by the surrounding 3.82 Ga gneisses. Pb isotope data for 00/22 are reported in Kamber et al. (2003).

2.2. Acasta gneisses, Slave Province, NWT, Canada

Sample SM/Ac/18 is a mafic biotite–plagioclase–garnet gneiss (SiO_2 ca. 43%) from the central part of the Acasta gneiss occurrence (Bowring et al., 1989; Bowring et al., 1990). The Acasta gneisses have yielded zircon U–Pb dates up to 4.03 Ga (Bowring and Williams, 1999) and are often quoted as the oldest rocks exposed on Earth. Bowring and Housh (1995) calculated initial $\varepsilon^{143}Nd$ based on an age of 4.0 Ga and reported values between −4.8 and +3.6 ε-units. However, Moorbath et al. (1997) published a ^{147}Sm–^{143}Nd regression age of 3371 ± 59 Ma for 25 samples of Acasta gneiss (including sample Ac/18) with an initial $\varepsilon^{143}Nd$ of -5.6 ± 0.7. This negative value, in combination with the oldest zircon date, clearly demonstrates the existence of some kind of ∼4.0-Ga-old precursor. But some doubt remains (see, for example, Kamber et al., 2001) whether the exposed Acasta gneiss is really 4.0 Ga old, or whether it is only 3.37 Ga old, in broad agreement with other reported regional ages. In any case, it is clear that the calculated initial $\varepsilon^{143}Nd$ values at 4.0 Ga cannot yield any useful information on mantle evolution at that time (for discussion, see Whitehouse et al., 2001).

2.3. Barberton komatiite, Kaapvaal craton, South Africa

This group comprises four mafic rock samples from the ca. 3.5 Ga Barberton greenstone belt, which represents the oldest preserved occurrence of komatiitic magmatism on Earth. Samples K5 and B25 are classified as tholeiitic basalts and samples 5085 and K27 as basaltic komatiites. Hamilton et al. (1979) published a well-defined whole-rock Sm–Nd isochron age of 3540 ± 30 Ma with an initial $\varepsilon^{143}Nd$ of 1.1 ± 0.7, in good agreement with the Pb–Pb age of 3497 ± 122 Ma obtained by Brévart et al. (1986).

3. Analytical techniques

3.1. Reproducibility of Nd isotope measurements

Previous attempts to detect ^{142}Nd anomalies in terrestrial rocks were severely limited by analytical difficulties related to the measurement of Nd isotope ratios with an external precision better than 15–20 ppm (2σ). Harper and Jacobsen (1992) and Goldstein and Galer (1992) first reported multidynamic measurements of the $^{142}Nd/^{144}Nd$ ratio with an external precision of 13 ppm (2σ) and

17 ppm (2σ), respectively, using a MAT262 thermal ionization mass spectrometer. Subsequently, Sharma et al. (1996) obtained $^{142}Nd/^{144}Nd$ static measurements with reproducibility of 15–20 ppm (2σ) using the same instrument and Regelous and Collerson (1996) reported a reproducibility of 19 ppm (2σ) for $^{142}Nd/^{144}Nd$ using a VG 54 TIMS. More recently, Boyet et al. (2003) measured $^{142}Nd/^{144}Nd$ by MC-ICPMS but also failed to reach external precision better than ≈15–20 ppm (2σ). Below we present evidence from repeated measurements of the Ames Nd standard ($N = 63$) acquired from March 2001 to January 2004 showing that the $^{142}Nd/^{144}Nd$ ratio can be determined with a long-term external precision of 2 ppm (2σ) using the Thermo Electron Triton new generation thermal ionization mass spectrometer. This represents an improvement by a factor of 5–10 compared with previous generations of mass spectrometers.

3.1.1. External precision of Nd standard measurements from march 2001 to August 2002

Instrumental mass fractionation precludes accurate determination of a given isotopic ratio unless a second ratio, stable and non-radiogenic, can be used for normalization. The final precision also depends on the fractionation law that is used to correct isotope fractionation during the evaporation process. Since the early work of Russell et al. (1978), the most commonly used fractionation law is the exponential law

$$\left(\frac{r_{ij}}{R^*_{ij}}\right) = \left(\frac{r_{kj}}{R^*_{kj}}\right)^{f_{ijk}}, \tag{1}$$

where r and R^* stand for measured and corrected ratio, respectively, and r_{ij} represents the ratio of two isotopes i and j of masses m_i and m_j. f_{ijk} is a mass-dependent fractionation factor, which can be expressed as a function of m_i, m_j, and m_k

$$f_{ijk} = \frac{\ln(m_i/m_j)}{\ln(m_k/m_j)}. \tag{2}$$

The normalization ratio r_{kj} is a ratio of stable non-radiogenic isotopes, whose value is fixed by convention. For Nd, it is common to use $R^*_{kj} = {}^{146}Nd/^{144}Nd = 0.7219$.

A first set of 33 standard measurements was acquired from March 2001 to August 2002 using the experimental procedure described in Caro et al. (2003a). External precision (2σ) for ratios corrected using the exponential law (Eqs. (1) and (2)) was 10 ppm for $^{142}Nd/^{144}Nd$, 6 ppm for $^{143}Nd/^{144}Nd$, 5 ppm for $^{145}Nd/^{144}Nd$, 15 ppm for $^{148}Nd/^{144}Nd$, and 30 ppm for $^{150}Nd/^{144}Nd$. However, as illustrated in Fig. 2, $^{142}Nd/^{144}Nd$, $^{148}Nd/^{144}Nd$, and $^{150}Nd/^{144}Nd$ ratios were shown to display strongly correlated variations ($r^2 = 0.6$–0.8) when plotted in binary diagrams (Caro et al., 2003a). Such residual correlations observed after application of the exponential law were shown to be consistent with a secondary, non-exponential, mass fractionation effect (Caro et al., 2003a). The slope defined by exponentially corrected ratios, in a r_{ij} versus r_{lj} normalized plot, is then given by the following equation (Albarède et al., 2004; Caro et al., 2003a,b; Galer and Abouchami, 2004):

$$A = \frac{\ln(m_i/m_j)\ln(m_i/m_k)}{\ln(m_l/m_j)\ln(m_l/m_k)}. \tag{3}$$

Note that the expression of A (Eq. (3)) is only a function of isotope masses. This implies that accurate correction of the effective mass fractionation process does not necessarily require the knowledge of the fractionation law that would ideally describe it, provided that it follows the general expression given by Eq. (1) and can be simply corrected by means of a second normalization ratio r_{lj} using the following equation:

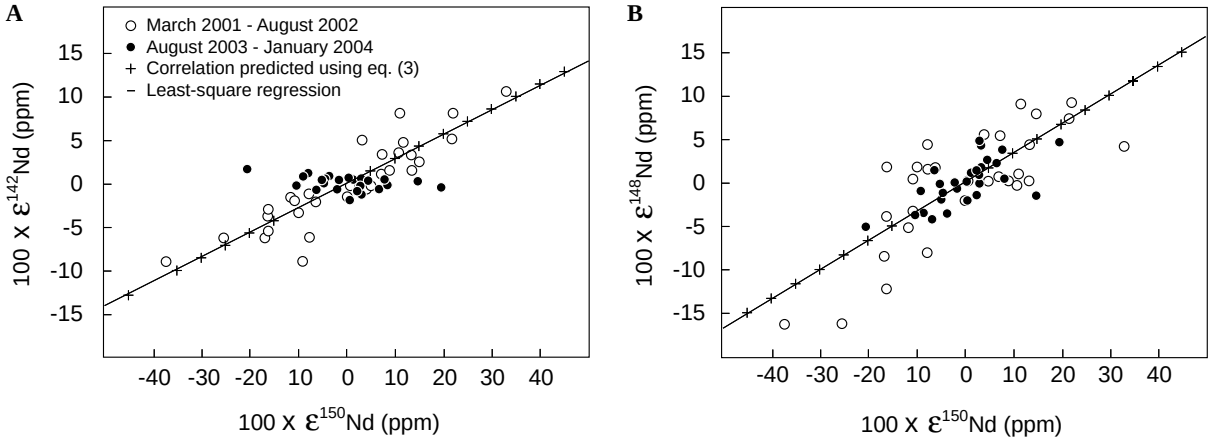

Fig. 2. Plot of (A) $\varepsilon^{142}Nd$ versus $\varepsilon^{150}Nd$ and (B) $\varepsilon^{148}Nd$ versus $\varepsilon^{150}Nd$ showing residual correlations observed after correction of instrumental mass fractionation using the exponential law. Data acquired after removal of the source magnet display no correlation in a $\varepsilon^{142}Nd$ versus $\varepsilon^{150}Nd$ plot. Note that a minor trend is still visible in a $\varepsilon^{148}Nd$ versus $\varepsilon^{150}Nd$ plot, reflecting larger error propagation on ratios with the largest mass difference. Note also the excellent agreement between slopes calculated using Eq. (3) and those estimated using a least-square regression. Error bars are omitted for the sake of clarity.

$$\left(\frac{r_{ij}}{R_{ij}}\right) = \left(\frac{r_{kj}}{R_{kj}}\right)^{f_{ijk}} \left(\frac{R^*_{lj}}{R_{lj}}\right)^{A}, \quad (4)$$

where R refers to the "true" isotopic ratios. In the ideal case where the exponential law perfectly describes the mass fractionation process, then $A = 0$ and $R = R^*$ for any isotopic ratio. R^*_{lj} refers to the second normalization ratio (here $^{150}Nd/^{144}Nd$) after correction from instrumental mass fractionation using the exponential law. Application of this double normalization procedure to our standard dataset obtained between January 2001 and August 2003 with $R_{kj} = {}^{146}Nd/^{144}Nd = 0.7219$ and $R_{lj} = {}^{150}Nd/^{144}Nd = 0.236431$ resulted in significant improvements in reproducibility for Nd ratios, with and external precision of 5 ppm (2σ) for $^{142}Nd/^{144}Nd$ and 8 ppm (2σ) for $^{148}Nd/^{144}Nd$ (Fig. 3).

3.1.2. External precision of Nd standard measurements between July 2003 and January 2004

An intriguing aspect of the observed secondary mass fractionation effect lies in its non-reproducibility. This is best demonstrated by the absence of correlation between measured and exponentially corrected ratios (Figs. 4A and B), as would be expected if the exponential law was systematically biased relative to the actual mass fractionation process. In addition, correlations with slopes predicted by Eq. (3) were also observed for Cr isotope measurements conducted over the same period of time by A. Trinquier and J.-L. Birck. These observations led us to consider the possibility of a secondary mass fractionation effect decoupled from the evaporation process. In particular, we investigated the effect on the Nd^+ beam of the electron deflection magnet located above the Z-deflection plates of the Triton focusing system (Fig. 5).

A second set of 30 Ames standard measurements was obtained from July 2003 to January 2004, after the magnet was removed from the Triton source. Results are given in Table 2 and plotted in Figs. 2 and 3. Note that all standard measurements acquired between July 2003 and January 2004 are included in Table 2, with the exception of NdAmes P4 and P19 whose acquisition was interrupted due to inaccurate filament positioning and large signal instabilities, respectively. Data were acquired using the procedure described in Section 3.3 and were corrected using the exponential law with $^{146}Nd/^{144}Nd$ as a normalization ratio (Eqs. (1) and (2)). External precision (2σ) of Nd isotope ratios was 2 ppm for $^{142}Nd/^{144}Nd$, 2 ppm for $^{143}Nd/^{144}Nd$, 3 ppm for $^{145}Nd/^{144}Nd$, 6 ppm for $^{148}Nd/^{144}Nd$, and 19 ppm for $^{150}Nd/^{144}Nd$ (Table 2), which represents an improvement by a factor of 5 compared with our first set of measurements corrected using the exponential law (Caro et al., 2003a). The absence of correlation between measured and corrected ratios (Fig. 4C) indicates that the exponential law adequately describes fractionation of Nd isotopes at the 1–2 ppm level of precision. The clear absence of correlation between ratios corrected using the exponential law (Fig. 2) is strongly suggestive that correlations displayed by our first standard dataset were related to the presence of the electron deflection magnet in the Triton ion source. This is further confirmed by the simultaneous vanishing of correlated variations observed between Cr isotope ratios (see above).

We hypothesize that the secondary mass fractionation effect described above can be interpreted as a combination

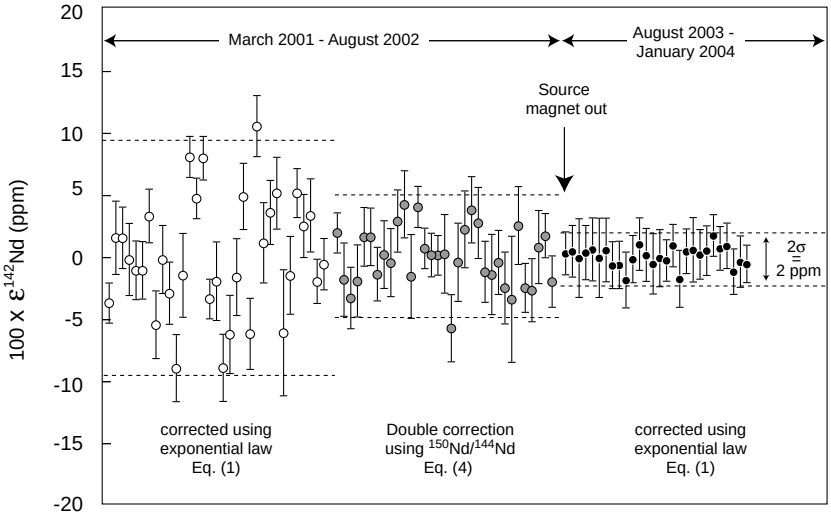

Fig. 3. Repeated measurements of the Nd Ames standard between March 2001 and January 2004. A first dataset acquired between March 2001 and August 2002 yielded external precision of ca. 10 ppm (2σ) when corrected using the exponential law (Eqs. (1) and (2)). Reproducibility was improved by a factor of 2 by using a double normalization procedure (Eqs. (3) and (4)). A second dataset was obtained between August 2003 and January 2004 after the electron-deflection magnet was taken out of the focusing lens stack of the mass spectrometer. This dataset yielded external precision of 2 ppm (2σ) when corrected using the exponential law, demonstrating the loss of precision related to the secondary mass fractionation effect induced by the source magnet. This represents an improvement by a factor 5–10 compared with former generations of mass spectrometers (e.g., Sharma et al., 1996). Error bars represent internal precision ($2\sigma_m$) of individual measurements.

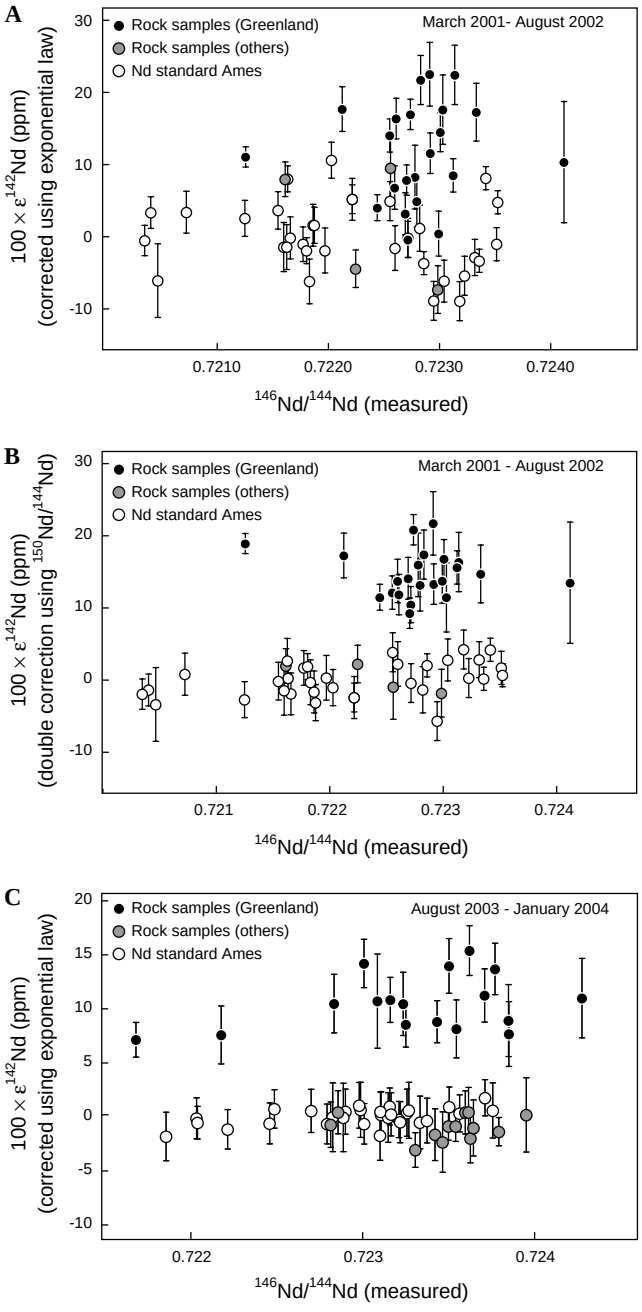

Fig. 4. Plot of ε^{142}Nd corrected from instrumental mass fractionation versus measured $^{146}Nd/^{144}Nd$ ratio. (A) Standard and rock sample measurements acquired between March 2001 and August 2002. Data are corrected from mass fractionation using the exponential law (Eqs. (1) and (2)). The lack of correlation in this diagram precludes a systematic bias between the effective mass fractionation process and the exponential law. (B) Same dataset corrected following the double normalization procedure outlined in the text (Eqs. (3) and (4)). (C) Standard and rock sample measurements acquired between August 2003 and January 2004, after removal of the ion source magnet. Data corrected using the exponential law do not exhibit correlations with measured ratios, suggesting that the exponential law correctly describes the instrumental mass fractionation process at the 2 ppm level of precision.

of two processes. First, the magnetic field generated by the source magnet produces a small deviation of the Nd^+ ion beam when it passes through focusing lenses, with the

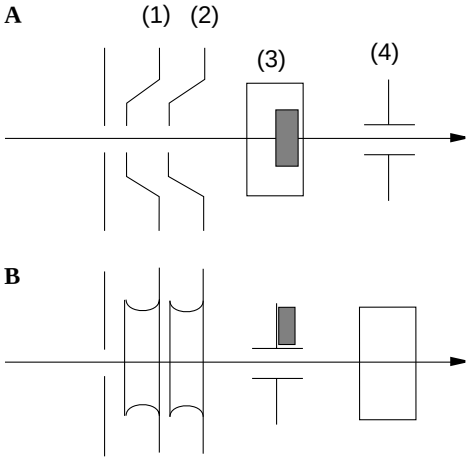

Fig. 5. Simplified scheme of the Triton focusing system (A) from above and (B) from side. (1) Extraction plates (right and left), (2) Condenser, (3) Z-focus, and (4) X-symmetry. The grey boxes show the location of the electron-deflection magnet. The arrows show the trajectory of the ion beam.

lighter ions being slightly more deflected than heavier ones. Second, the resulting lateral isotopic heterogeneity of the beam translates to a non-ideal mass fractionation when a fraction of the beam is lost at the source exit slit. Because of the location of the magnet within the focusing lens stack, there is a dependence of the magnitude of this secondary mass fractionation effect on focus parameters, which accounts for the non-reproducibility of mass fractionation from one sample to the next.

Elimination of the double normalization procedure resulted in significant improvements of Nd isotope ratio reproducibility (Fig. 3), which subsequently led us to refine our first estimate of the $^{142}Nd/^{144}Nd$ anomaly in Isua metasediments (see Section 4). However, both datasets yield consistent results regarding the presence of a positive $^{142}Nd/^{144}Nd$ anomaly in our samples. This agreement definitely precludes a possible analytical bias arising from our double normalization procedure. Rather, it validates its use in removing mass fractionation effects resulting from small deviations between correction laws and the actual instrumental mass fractionation.

3.2. Nd chemical separation

Rock sample aliquots of 50–100 mg were dissolved in HF 50% + 16 M HNO_3 in Savillex Teflon vials and heated at 140 °C for 24 h in a temperature-controlled oven. Although no residual grains were observed following dissolution, zircons contained in felsic metasediments and orthogneisses may have experienced only partial dissolution using this method. Zircons typically have high $^{147}Sm/^{144}Nd \approx 1$) and in situ radioactive decay of ^{146}Sm in 3.8-Gyr-old zircons is therefore expected to produce small ^{142}Nd excesses (<5 ppm) over the initial bulk rock value (Amelin, 2004). However, considering a maximum Zr content of 1000 ppm (i.e., 0.2 wt% zircon) and a

maximum Nd concentration in zircons of ≈10 ppm (Amelin, 2004), in situ decay of ^{146}Sm would only increase the $^{142}Nd/^{144}Nd$ ratio in a 3.8-Gyr-old rock by 0.1 ppm, well below the resolution of our measurements. Therefore, incomplete dissolution of zircons is extremely unlikely to have biased the measured ^{142}Nd signature of our samples.

After evaporation, residues were dissolved in 3 ml of 3 M HNO_3 and heated at 100 °C for 2 h. Boric acid (20–40 mg) was then added and the solutions were gently heated at 80 °C for 3–5 h to ensure complete redissolution of Mg and Ca fluorides. Separation of REE from the rock matrix was performed using 500 μl TRU-Spec chromatographic columns. The TRU-Spec resin allows extremely selective separation of REE, with excellent elimination of Ba. However, prior to loading on the column, Fe must be reduced to avoid competition between trivalent Fe and REE. Addition of 30 mg ascorbic acid usually ensures reduction of Fe from a 100 mg basalt sample. Complete Fe reduction was checked by addition of one drop of ammonium thiocyanate, which turns dark red in the presence of trivalent iron. Samples were then centrifuged to check complete dissolution of the rock powder and absence of precipitates. Each new batch of TRU-Spec resin was first washed twice in 2 M HNO_3 and distilled H_2O, and preconditioned with 3 ml of 3 M HNO_3. Sample solutions were introduced in 3 ml of 3 M HNO_3. Most matrix constituents were washed with 6 ml of 2 M HNO_3 and the REE fraction was eluted in 3 ml H_2O. Because TRU spec resins were shown to have strong memory effects, even after thorough washing with HNO_3 and H_2O, batches of resin were systematically discarded after each use.

A major requirement of the ^{142}Nd chemistry is to efficiently separate Ce from Nd to reduce the $^{142}Ce/^{142}Nd$ ratio from a value of ≈1 in crustal rocks to about 10^{-6}. This requirement is usually not fulfilled by standard Nd chemistry involving di(2-ethylhexyl) orthophosphoric acid (HDEHP) extraction chromatography (Rehkämper et al., 1996), and further purification of Ce from REE is required. The chemical procedure used in this study is a liquid–liquid extraction involving oxidation of Ce into its tetravalent state by a strongly oxidizing agent and preferential complexation of Ce^{4+} by an organic extractant. Only a brief outline of the method is given here. For further details, the reader is referred to Rehkämper et al. (1996). Samples are first dissolved in 500 μl of an oxidizing solution of 5 mM $NaBrO_3$ in 10 M HNO_3. The organic extractant consists of 3 M HDEHP in *n*-heptane. The aqueous solution containing REE^{3+} and oxidized Ce^{4+} is introduced with 500 μl of organic phase into a 2 ml centrifuge tube and shaken manually for 3 min. The organic phase is then discarded and the procedure repeated twice using new batches of 3 M HDEHP in *n*-heptane. The aqueous solution is then purified from remaining traces of dissolved HDEHP and complexed Ce^{4+} by 3 agitation steps of 3 min each with pure *n*-heptane. Trivalent REE are then recovered by pipetting out the aqueous solution from the bottom of the tube. This extraction step ensures purification of Ce from other REE with a separation coefficient better than 10^3.

The use of large amounts of Na bromate requires elimination of abundant Na from the REE fraction prior to Nd separation. For this step, a cation exchange resin was preferred over the TRU-Spec resin since the use of the latter was shown to induce important (30–50%) losses of REE, probably related to the presence of residual HDEHP in the aqueous solution. Samples were dissolved in 200 μl of 2 M HCl and introduced in 2 ml AG50-X8 chromatographic columns. Na was washed in 12 ml of 2 M HCl and REE eluted with 3 ml of 4 M HCl.

The REE fraction was then dissolved in 200 μl of 0.21 M HCl and loaded on a 2 ml HDEHP LN-Spec extraction chromatographic column. Typical elution volumes for La–Ce–Pr were 15 ml. Nd was then recovered in 4 ml of 0.24 M HCl. The Ce–Nd separation coefficient for this step is about 10^2–10^3. Overall, the separation factor was better than 10^6, thereby reducing the $^{142}Ce/^{142}Nd$ ratio to less than about 1–5 ppm. Note also that Sm–Nd separation using the HDEHP chromatographic column resulted in $^{144}Sm/^{144}Nd$, $^{148}Sm/^{148}Nd$, and $^{150}Sm/^{150}Nd$ ratios usually less than 10^{-7}, such that corrections for Sm isobaric interferences were not needed.

Total procedural blanks were 50–100 pg Nd and chemistry yields were >80%.

3.3. Mass spectrometry

The precision achievable for Nd isotope ratios using the Triton (Fig. 3) represents an improvement by a factor of 5–10 compared with previous generations of mass spectrometers (e.g., Sharma et al., 1996). While the reproducibility of Nd isotope ratios obtained using the MAT262 thermal-ionization mass spectrometer was shown to be limited by ion optic and amplifier calibrations (Sharma et al., 1996), our results indicate that none of the above sources of error significantly alter the reproducibility of Nd isotope ratios using Triton. Below we detail the analytical procedure used to measure Nd isotope ratios of standard and samples and discuss the main sources of error that can potentially affect our measurements.

Nd (300–500 ng) was dissolved in 1 μl of 6 M HCl and loaded on outgassed zone-refined rhenium by heating with a 0.8 A current. Sample loads were then slowly heated at ca. 1.3 A and 1 μl of 0.01% phosphoric acid was added. The filaments were then heated to dull red at ca. 1.8–2 A over a few seconds.

Nd was run as the metal ion using a double rhenium filament assembly. The ionization filament was first heated at a rate of 200 mA/min to a temperature of 1650 °C. The evaporation filament was then heated at 100 mA/min until a signal of 10^{-12} A was obtained. The beam was centered and roughly focused and the evaporation filament was slowly heated to obtain an ion current of $4–5 \times 10^{-11}$ A for ^{142}Nd. The beam was refocused until an optimum intensity was reached.

Table 1
Multidynamic acquisition scheme for Nd isotope measurements

Cup #	L3	L2	L1	CC	H1	H2	H3	H4	Focus quad (V)	Disp. quad (V)
Line 1	^{142}Nd	^{143}Nd	^{144}Nd	^{145}Nd	^{146}Nd	^{147} Sm	^{148}Nd	^{150}Nd	−2	−3.5
Line 2	—	^{142}Nd	^{143}Nd	^{144}Nd	^{145}Nd	^{146}Nd	^{147}Sm	^{149}Sm	−2	0
Line 3	^{140}Ce	—	^{142}Nd	^{143}Nd	^{144}Nd	^{145}Nd	^{146}Nd	^{148}Nd	−2	3

The presence of ion optics effects related to the focusing settings on Z-focus plates was shown by Sharma et al. (1996) to significantly contribute to the dispersion of $^{142}Nd/^{144}Nd$ measurements using the MAT262. Although no such effects were identified using the Triton, all samples and standards were focused using a unique standard procedure. Extraction plates (right and left, see Fig. 5) were, respectively, set at 9100 and 9000 V. These parameters correspond to optimum focus settings determined using the "Auto-full range" procedure of the Triton software. The 100 V difference is linked to the curved shape of the ion beam trajectory due to the use of a double filament assembly and probably also to a residual mechanical tolerance from the source construction. The potential of the condenser plate (Fig. 5) was set to achieve the best signal intensity. Extraction plates and condenser were focused repeatedly until no gain of signal was obtained. Finally, the beam was refocused using the Triton automatic procedure, including focusing of *X*-symmetry and Z-focus deflection lenses (Fig. 5), until optimum intensity was achieved. In most cases, the potentials applied on deflection plates were small (−20 to +20 V). Nevertheless, inaccurate positioning of the filament assembly may occasionally result in larger voltage on Z-focus plates. In this case, both *X*-symmetry and Z-focus were reset to zero and the beam focused using the sample wheel *Z*-positioning system, allowing better vertical alignment of the emitting spot in the optical axis of the mass spectrometer. *X*-symmetry and *Z*-focus were then refocused. This method usually reset the voltage applied to *Z*-deflection plates to more moderate values.

The absence of a Nd isotope lighter than ^{142}Nd does not allow the use of a ratio bracketing ^{142}Nd and ^{144}Nd to correct measured $^{142}Nd/^{144}Nd$ ratios for instrumental mass fractionation. We have therefore applied the conventional exponential law correction using $^{146}Nd/^{144}Nd$ as a normalizing ratio. Since ^{146}Nd is located on the heavy mass side of the instrument, any asymmetry in the ion beam optical characteristics with respect to the optical axis of the mass spectrometer could produce artifacts during correction of $^{142}Nd/^{144}Nd$ ratios for instrumental mass fractionation. These, however, can be identified by measuring Nd using different cup configurations. In this study, the use of a multidynamic scheme was therefore preferred to static multicollection. Measurements were performed using 3 configurations, with ^{145}Nd, ^{144}Nd, and ^{143}Nd successively collected in the central cup (Table 1). Line 1 (^{145}Nd in central cup) is identical to the static configuration used in Caro et al. (2003a). The potentials applied to the two quadrupoles located at the entrance of the flight tube (Focus quad) and at the exit of the magnet (Dispersion quad) were adjusted to ensure precise coincidence of Nd ion beams with their respective cups for the three acquisition lines and to improve peak shapes. Note that quadrupole parameters were finely tuned for each sample. The $^{142}Nd/^{144}Nd$ reproducibility achieved for each acquisition line was approximately 4–6 ppm (2σ), which does not significantly exceed the internal precision of individual measurements. In all cases, the magnitude of ^{142}Nd anomalies was shown to be identical within errors for each configuration, suggesting no significant asymmetry in the mass spectrometer optical characteristics with respect to its optical axis.

As illustrated in Fig. 3, the external precision (2σ) achieved for $^{142}Nd/^{144}Nd$ ratio is essentially identical to the internal precision ($2\sigma_m$) of individual measurements (≈2 ppm, Table 3).The latter is, in turn, only slightly higher than the theoretical counting error predicted by Poisson statistics (≈1–1.5 ppm). This suggests that the major source of error at the level of precision considered in this study is related to ion-counting statistics, at least for ratios with small relative mass difference (i.e., $^{142}Nd/^{144}Nd$, $^{143}Nd/^{144}Nd^{145}Nd/^{144}Nd$). This, in turn, has led us to maximize acquisition time in order to decrease the ion counting error down to negligible levels. As a consequence, measurements are typically 10–12 h long (corresponding to 7–9 h counting). Although a similar result could be theoretically achieved by increasing ion beam intensity, we chose to use moderate signals ($3–5 \times 10^{-11}$ A for ^{144}Nd, see Tables 2 and 3) as more intense beams were shown to significantly alter the stability of evaporation. Each measurement was composed of 36–54 blocks comprising 10 cycles. Each cycle was composed of 3 sub-cycles corresponding to the three acquisition lines shown in Table 1. Each sub-cycle comprises 16 integrations (equivalent to ca. 16 s acquisition time) and is preceded by an idle time of 4 s. Integrations were filtered at 3σ. Relative gains between amplifiers (66 s integration) were calibrated each 27 blocks and baselines (33 s integration) were measured after each block. The ion beam was centered and refocused every 3 blocks. Ion yields are typically 3%. Ce isobaric interference at mass 142 was monitored using the $^{140}Ce/^{144}Nd$ ratio measured on line 3 (Table 1) and $^{142}Ce/^{142}Nd$ ratios for rock samples were in most cases found to be negligible (Table 3). Note that due to the long counting time involved in sample measurements, the $^{140}Ce/^{144}Nd$ ratio can be determined using Faraday cup with a precision typically below 1‰, thereby allowing accurate correction of $^{142}Nd/^{144}Nd$ ratios for isobaric interfer-

Table 2
Analytical results for Nd standard Ames obtained between August 2003–January 2004[a]

NdAmes N	Date	^{144}Nd (10^{-11} A)	^{142}Nd/^{144}Nd	$2\sigma_m$ (ppm)	^{143}Nd/^{144}Nd	$2\sigma_m$ (ppm)	^{145}Nd/^{144}Nd	$2\sigma_m$ (ppm)	^{148}Nd/^{144}Nd	$2\sigma_m$ (ppm)	^{150}Nd/^{144}Nd	$2\sigma_m$ (ppm)	^{146}Nd/^{144}Nd	^{142}Ce/^{142}Nd (ppm)
P1	27/07/03	3.26	1.1418385	1.7	0.5119607	1.5	0.3484054	1.3	0.2415813	2.9	0.2364537	5.3	0.723066	<1
P2	28/07/03	2.80	1.1418387	2.1	0.5119601	1.7	0.3484042	1.6	0.2415803	3.4	0.2364517	6.6	0.722401	4
P3	31/07/03	3.69	1.1418381	3.2	0.5119600	2.5	0.3484046	2.1	0.2415805	4.7	0.2364536	9.5	0.722389	1
P5	1/08/03	3.90	1.1418386	2.2	0.5119599	1.9	0.3484048	1.7	0.2415800	3.6	0.2364564	7.1	0.722760	<1
P6	2/08/03	3.57	1.1418389	2.5	0.5119603	2.2	0.3484038	2.0	0.2415815	4.1	0.2364536	8.2	0.722489	2
P7	4/08/03	3.49	1.1418381	3.2	0.5119602	2.6	0.3484043	2.4	0.2415805	5.0	0.2364549	10.1	0.722328	2
P8	4/08/03	4.19	1.1418388	2.6	0.5119604	2.1	0.3484044	1.8	0.2415813	3.9	0.2364548	7.0	0.723258	<1
P9	5/08/03	3.05	1.1418374	1.9	0.5119602	1.6	0.3484053	1.4	0.2415800	3.0	0.2364535	5.5	0.722511	<1
P10	20/08/03	4.70	1.1418374	1.9	0.5119603	1.6	0.3484049	1.4	0.2415807	3.0	0.2364515	5.8	0.721961	<1
P11	20/08/03	4.19	1.1418360	2.2	0.5119603	1.9	0.3484046	1.6	0.2415793	3.8	0.2364513	6.8	0.721358	<1
P12	22/08/03	4.41	1.1418380	1.9	0.5119607	1.7	0.3484044	1.4	0.2415795	3.1	0.2364505	6.2	0.721535	<1
P13	23/08/03	4.18	1.1418393	2.1	0.5119604	1.8	0.3484043	1.6	0.2415795	3.2	0.2364509	6.2	0.722482	<1
P14	25/08/03	4.42	1.1418383	2.1	0.5119609	1.8	0.3484050	1.6	0.2415799	3.3	0.2364518	6.6	0.722609	<1
P15	13/09/03	5.36	1.1418375	2.4	0.5119606	2.0	0.3484043	1.7	0.2415804	3.6	0.2364525	7.8	0.722836	<1
P16	14/09/03	3.44	1.1418380	2.3	0.5119600	1.9	0.3484044	1.6	0.2415808	3.6	0.2364537	6.8	0.722650	<1
P17	27/09/03	4.27	1.1418378	1.7	0.5119607	1.5	0.3484051	1.3	0.2415807	2.7	0.2364535	5.0	0.722713	<1
P18	28/09/03	4.21	1.1418392	1.7	0.5119601	1.5	0.3484047	1.3	0.2415795	2.8	0.2364521	5.3	0.722659	<1
P20	24/10/03	4.70	1.1418361	2.3	0.5119595	1.9	0.3484039	1.7	0.2415798	4.0	0.2364530	7.4	0.722603	<1
P21	26/10/03	4.70	1.1418387	1.8	0.5119607	1.5	0.3484041	1.4	0.2415802	3.1	0.2364525	5.7	0.722605	<1
P22	27/10/03	4.68	1.1418388	2.6	0.5119610	2.0	0.3484048	1.8	0.2415801	4.1	0.2364519	6.5	0.722770	<1
P23	28/10/03	4.81	1.1418384	2.0	0.5119600	1.7	0.3484050	1.5	0.2415809	3.1	0.2364540	5.9	0.722667	<1
P24	29/10/03	4.90	1.1418388	2.0	0.5119605	1.7	0.3484053	1.6	0.2415806	3.1	0.2364532	6.2	0.722202	<1
P25	30/12/03	4.08	1.1418401	1.7	0.5119606	1.3	0.3484055	1.4	0.2415791	2.5	0.2364481	4.3	0.723213	<1
P26	1/01/04	5.97	1.1418389	1.8	0.5119611	1.5	0.3484049	1.4	0.2415804	2.8	0.2364530	5.3	0.721988	<1
P27	2/01/04	4.97	1.1418392	1.8	0.5119609	1.5	0.3484049	1.4	0.2415801	2.8	0.2364508	5.6	0.723005	<1
P28	3/01/04	5.46	1.1418374	1.8	0.5119599	1.5	0.3484048	1.3	0.2415784	3.1	0.2364479	5.6	0.722294	<1
P29	5/01/04	5.73	1.1418368	1.8	0.5119599	1.5	0.3484043	1.4	0.2415803	3.0	0.2364536	5.4	0.721716	<1
P30	6/01/04	5.42	1.1418377	2.1	0.5119600	1.7	0.3484042	1.6	0.2415815	3.3	0.2364575	6.3	0.722876	<1
P31	7/01/04	4.93	1.1418375	1.5	0.5119599	1.2	0.3484041	1.1	0.2415809	2.4	0.2364545	4.5	0.721541	<1
P32	10/01/04	5.38	1.1418376	1.9	0.5119607	1.7	0.3484043	1.5	0.2415819	3.0	0.2364581	6.0	0.722720	<1
Average			1.1418382		0.5119604		0.3484046		0.2415803		0.2364529			
Reproducibility (2σ)			2 ppm		2 ppm		3 ppm		6 ppm		19 ppm			

Uncertainties represent internal precision of each measurement ($2\sigma_m$).
[a] Data acquired consecutively over the same period as the rock samples.

Table 3
Analytical results for early Archaean rocks and modern oceanic basalts[a]

	Date	^{144}Nd (10^{-11} A)	^{142}Nd/^{144}Nd	$100 \times \varepsilon^{142}$Nd	$2\sigma_m$ (ppm)	^{143}Nd/^{144}Nd	$2\sigma_m$ (ppm)	^{145}Nd/^{144}Nd	$2\sigma_m$ (ppm)	^{148}Nd/^{144}Nd	$2\sigma_m$ (ppm)	^{150}Nd/^{144}Nd	$2\sigma_m$ (ppm)	^{146}Nd/^{144}Nd	^{142}Ce/^{142}Nd (ppm)
Metasediments															
248443	05/01/04	3.15	1.1418557	15.4	2.3	0.5135102	1.9	0.3484053	1.7	0.2415809	3.6	0.2364535	7.1	0.72312	<1
248484A	31/07/03	3.69	1.1418468	7.6	2.7	0.5107471	2.2	0.3484048	2.0	0.2415800	4.2	0.2364515	8.3	0.72168	<1
SM/GR/93/13	03/08/03	2.83	1.1418507	11.0	3.7	0.5118026	3.1	0.3484055	2.8	0.2415789	6.0	0.2364499	12.3	0.72378	<1
SM/GR/93/33	04/01/04	4.02	1.1418541	13.9	2.5	0.5124038	2.2	0.3484043	1.8	0.2415807	3.9	0.2364556	7.2	0.72300	4
SM/GR/93/57	03/01/04	6.05	1.1418482	8.8	1.9	0.5110099	1.7	0.3484050	1.6	0.2415797	3.2	0.2364497	6.2	0.72294	<1
SM/GR/97/31	01/01/04	4.83	1.1418543	14.2	2.2	0.5107282	2.0	0.3484053	1.7	0.2415792	3.7	0.2364514	6.6	0.72251	3
SM/GR/99/15	21/08/03	3.30	1.1418510	11.2	2.5	0.5106849	2.1	0.3484054	1.8	0.2415804	3.9	0.2364517	7.6	0.72321	5
Orthogneisses															
155702	26/10/03	3.44	1.1418469	7.6	3.0	0.5111712	2.5	0.3484047	2.3	0.2415805	4.8	0.2364570	9.8	0.72335	<1
155706	25/10/03	4.58	1.1418463	7.1	1.6	0.5104629	1.4	0.3484044	1.3	0.2415788	2.9	0.2364476	5.4	0.72118	<1
155768	14/09/03	4.26	1.1418474	8.1	2.7	0.5113747	2.2	0.3484044	2.0	0.2415797	4.0	0.2364553	7.6	0.72305	<1
155774	29/09/03	3.08	1.1418483	8.9	3.3	0.5104245	2.7	0.3484048	2.5	0.2415792	5.2	0.2364505	10.1	0.72335	2
SM/GR/98/2	27/10/03	4.35	1.1418479	8.5	2.1	0.5102049	1.8	0.3484050	1.7	0.2415784	3.6	0.2364468	6.7	0.72275	<1
Metabasalts															
SM/GR/98/21	19/08/03	3.16	1.1418501	10.5	2.7	0.5127964	2.3	0.3484043	2.1	0.2415798	4.5	0.2364535	9.0	0.72234	<1
SM/GR/98/23	24/08/03	3.49	1.1418505	10.8	2.1	0.5129935	1.8	0.3484044	1.6	0.2415809	3.5	0.2364540	6.7	0.72266	<1
SM/GR/98/23 (d)	21/08/03	3.42	1.1418501	10.4	2.9	0.5130060	2.6	0.3484047	2.2	0.2415784	4.7	0.2364488	9.4	0.72274	2
SM/GR/98/26	05/08/03	3.11	1.1418504	10.7	4.4	0.5125976	4.0	0.3484056	3.4	0.2415791	7.3	0.2364565	13.7	0.72259	1
Amphibolite enclave															
SM/GR/00/22	27/09/04	3.52	1.1418538	13.7	2.4	0.5129540	2.1	0.3484053	1.7	0.2415796	3.6	0.2364522	7.6	0.72327	4
Acasta															
SM/Ac/18	11/01/04	5.89	1.1418365	−0.9	1.3	0.5104468	1.7	0.3484055	1.1	0.2415798	3.3	n.m.	—	0.72300	<1
Barberton komatiite															
B25	02/01/04	4.20	1.1418362	−1.7	2.4	0.5123430	2.0	0.3484057	1.7	0.2415793	3.8	0.2364487	7.3	0.72292	2
5085	31/12/03	5.27	1.1418386	0.4	2.0	0.5126941	1.7	0.3484056	1.4	0.2415786	2.9	0.2364483	5.7	0.72310	5
K27	03/08/03	3.79	1.1418373	−0.8	2.1	0.5123441	1.8	0.3484053	1.6	0.2415795	3.7	0.2364512	6.6	0.72232	<1
K27 (d)	31/12/03	4.92	1.1418366	−1.4	1.3	0.5123502	1.8	0.3484035	1.3	0.2415826	3.2	n.m.	—	0.72329	1
K5	31/10/03	3.35	1.1418355	−2.4	2.8	0.5123587	2.5	0.3484052	2.2	0.2415800	4.6	0.2364559	8.4	0.72297	<1
K5 (d)	30/12/03	4.32	1.1418372	−0.9	1.4	0.5123738	4.4	0.3484051	4.1	0.2415802	16.0	n.m.	—	0.72304	1
Pitcairn															
PN3-10	08/01/04	5.11	1.1418358	−2.0	2.3	0.5126213	2.0	0.3484047	1.7	0.2415795	3.7	0.2364533	7.1	0.72313	1
PN8-4	31/10/03	3.42	1.1418369	−1.1	2.6	0.5124307	2.1	0.3484055	2.0	0.2415802	4.0	0.2364526	7.3	0.72315	6
Society															
PN20-13	09/01/04	3.98	1.1418347	−3.1	1.6	0.5126028	5.1	0.3484039	4.7	0.2415793	18.0	n.m.	—	0.72281	<1
PN20-5	08/01/04	4.10	1.1418387	0.4	2.3	0.5128165	4.7	0.3484047	6.2	0.2415802	9.8	n.m.	—	0.72312	<1
Mid ocean ridge basalts															
MD37-D3	11/01/04	4.23	1.1418387	0.4	2.0	0.5126151	3.8	0.3484041	5.3	0.2415820	7.9	n.m.	—	0.72236	2
Mapco DR11-A	16/09/03	2.85	1.1418383	0.2	3.4	0.5132036	2.9	0.3484053	2.7	0.2415786	5.4	0.2364488	10.5	0.72345	5

Uncertainties represent internal precision of each measurement ($2\sigma_m$). d, duplicate dissolutions; n.m., not measured.
[a] Data acquired consecutively over the same period as the standard data.

ence. Tests conducted at regular intervals between August 2003 and January 2004 did not reveal significant differences between $^{140}Ce/^{144}Nd$ ratios measured using Faraday cups (in the static mode) and ion multiplier (in the dynamic mode).

Previous attempts to measure Nd isotope ratios at high precision using the MAT 262 mass spectrometer were hampered by the uncertainty on the relative gains of the amplifiers. In particular, Sharma et al. (1996) showed that the reproducibility of gain calibrations measured over a period of 12 h was approximately 9 ppm (2σ), thereby limiting the external precision of Nd isotope measurements achievable using MAT262. In this study, we have used the "amplifier rotation" system available on Triton. This system allows switching amplifiers/Faraday cup connections between each block such that each cup is successively connected to each amplifier. The uncertainty relative to gain calibration is then cancelled by adding errors on gain values for the 9 amplifiers. Although the uncertainty related to gain calibration is difficult to estimate when the amplifier rotation mode is used, our data suggest that it represents a source of error smaller than the uncertainty related to ion counting. It may be noted that the multidynamic acquisition scheme also plays, to some extent, the role of amplifier rotation. However, the latter is expected to be more efficient in eliminating uncertainties on gain calibrations as it averages calibration errors for 9 amplifiers, against 3 for the multidynamic acquisition method (Table 1). The data were therefore acquired by combining amplifier rotation with a multidynamic acquisition scheme. Note that amplifier rotation is done between each block such that a complete sequence of rotation corresponds to 9 blocks. In contrast, peak-switching is done between each sub-cycle and isotopic ratios measured in three different configurations (Table 1) are averaged for each cycle.

4. Results

All rock samples were analyzed between August 2003 and January 2004 following the experimental procedure presented in Section 3. Measurements were usually performed over 7 day sessions, which allowed systematic bracketing of rock samples with measurements of the Nd Ames standard. Table 3 gives the results of early Archaean rocks from Acasta, West Greenland, and Barberton, and various modern oceanic basalts. As mentioned in Section 2, the reproducibility of standard measurements is essentially controlled by ion counting statistics, at least for ratios with a small mass difference (i.e., $^{142}Nd/^{144}Nd$, $^{143}Nd/^{144}Nd$, and $^{145}Nd/^{144}Nd$). Hence, in order to keep internal consistency between standard and rock sample data, we systematically discarded runs whose signal was insufficient to obtain internal precision better than ≈4 ppm for $^{142}Nd/^{144}Nd$. The uncertainty associated with each isotopic ratio (internal precision) is defined as $2\sigma_m = 2\sigma/\sqrt{n}$, where σ is the standard deviation and n is the number of cycles. The uncertainties given below for metabasalts, orthogneisses, and Barberton samples are given as 2σ (duplicates are not included in error calculations). Results for $^{142}Nd/^{144}Nd$ are summarized in Fig. 6.

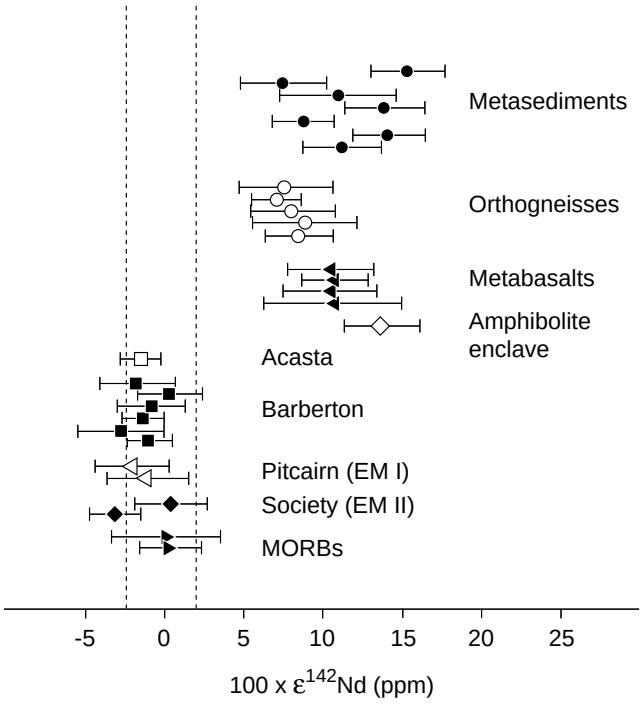

Fig. 6. $\varepsilon^{142}Nd$ results for Archean rocks from West Greenland, Barberton, and Acasta, and modern oceanic basalts. Rock sample measurements were systematically bracketed with analyses of the Nd Ames standard. All rock samples from the West Greenland craton display well-defined ^{142}Nd excesses compared to modern oceanic basalts and Ames Nd standard. Note that all data from Table 3 are represented (including duplicates). Error bars represent the internal precision of individual measurements ($2\sigma_m$).

Our new ^{142}Nd results indicate that metabasalts, metasediments, and orthogneisses from the early Archaean Greenland craton carry ^{142}Nd anomalies ranging between 7.6 ± 2.7 and 15.2 ± 2.3 ppm ($2\sigma_m$). Note that there is no discrepancy between the data reported here and the preliminary study by Caro et al. (2002) showing no ^{142}Nd anomaly in 2 Isua and 1 Amîtsoq samples (of unknown location). Indeed, the lower precision of these preliminary measurements did not allow the detection of the small anomalies reported here. Because radioactive decay of ^{146}Sm is negligible after ca. 4.2 Ga, the existence of positive ^{142}Nd anomaly in early Archaean mantle demonstrates that the Earth's mantle experienced Sm/Nd fractionation at an early stage of its evolution. In contrast, modern oceanic basalts from Pitcairn (EMI), Society (EMII), as well as two MORB samples, have $^{142}Nd/^{144}Nd$ ratios indistinguishable from the Ames Nd standard value. This suggests that early differentiated reservoirs were extensively rehomogenized over the past 4.0 billion years, leaving no remnants of an early Sm/Nd fractionation in the present-day mantle. Below we discuss the essential features characterizing ^{142}Nd systematics of early Archaean rocks from West Greenland, Acasta, and Barberton.

4.1. Southern West Greenland

4.1.1. Metamorphosed basaltic rocks from the Isua greenstone belt

Metabasalts exhibit positive ^{142}Nd anomalies averaging 10.7 ± 0.3 ppm (2σ) (Fig. 6). No significant variations are observed between different samples or between cores (98/26) and rims (98/23) of pillows. In contrast, Boyet et al. (2003) analyzed eight Isua metabasalts using ICP-MS and reported anomalies as high as 30 ± 20 ppm (2σ) in three samples, whereas five other samples were shown to carry no detectable anomaly at this level of precision. These results were then confirmed by Boyet and Carlson (2004) using more precise Triton analyses. Such heterogeneity among rocks sampled within a relatively small geographic area is unexpected and was interpreted by Boyet et al. (2003) as reflecting remobilization of Nd by metamorphic fluid during late Archaean. However, this hypothesis is contradicted by the homogeneous ^{142}Nd signature of the metabasalts presented here. Polat et al. (2003) demonstrated that the ^{147}Sm–^{143}Nd system was reset as late as 2.57 Ga in pillowed metabasalts, with rims generally more disturbed than cores. However, it is evident that samples 98/26 (core) and 98/23 (rim) still retain a significant and homogeneous ^{142}Nd anomaly. This suggests that $^{142}Nd/^{144}Nd$ systematics of Isua metabasalts have not been significantly disturbed by post-emplacement alteration and metamorphic processes. The uniform $\varepsilon^{142}Nd$ value of 10.7 ± 0.3 ppm (2σ) of these metabasalts may therefore represent the closest approximation in our entire dataset to the contemporaneous mantle source region. The greater dispersion of $\varepsilon^{142}Nd$ data of metasediments probably reflects the more complex provenance of these rocks, involving greater opportunity for mixing of different crustal protoliths.

4.1.2. Gneisses of magmatic origin (orthogneisses)

Four samples of ca. 3.65 Ga orthogneisses exhibit homogeneous $^{142}Nd/^{144}Nd$ anomalies averaging 7.9 ± 1.5 ppm (2σ) (Fig. 6). In addition, one sample of ca. 3.81 Ga orthogneiss has $100 \times \varepsilon^{142}Nd = 8.5 \pm 2.1$ ppm ($2\sigma_m$). Accordingly, 3.65 Ga gneisses appear slightly less radiogenic than metabasalts, although the difference between the two sample populations is too small to be resolved at the 95% level of confidence. It is not clear whether this small, but probably significant, difference in $\varepsilon^{142}Nd$ between the basalts and the orthogneisses results from different mantle sources, or from an admixture of mantle and crust components, in the genesis of the gneisses.

4.1.3. Metamorphosed clastic sediments from the Isua greenstone belt

^{142}Nd anomalies with values between 7.6 ± 2.7 ppm ($2\sigma_m$) and 15.4 ± 2.3 ppm ($2\sigma_m$) are observed in metasediments from the northeastern sector of the IGB (Fig. 6). These new results are consistent within errors with our initial report of positive $\varepsilon^{142}Nd$ anomalies in Isua metasediments (Caro et al., 2003a), although our new analyses yield a slightly lower average value than initially inferred from our first (less precise) dataset (Fig. 7). It is emphasized, however, that our new metasediment dataset is not strictly identical to the dataset presented in Caro et al. (2003a). Examination of measurements for the five samples common to Caro et al. (2003a) and this study suggests that our initial estimate could be overestimated by 3.5 ppm. Note, however, that this small difference is below the external precision of measurements from Caro et al. (2003a) ($2\sigma = 5$ ppm). Note also that the observed dispersion of our new metasediment dataset clearly exceeds analytical scatter, suggesting that metasediments may represent a heterogeneous formation with respect to $^{142}Nd/^{144}Nd$ ratio. Since igneous rocks appear to have retained homogeneous ^{142}Nd signature despite metamorphic processes, $^{142}Nd/^{144}Nd$ heterogeneity in Isua metasediments would be best explained by contribution of different rock sources with variable $^{142}Nd/^{144}Nd$ signature.

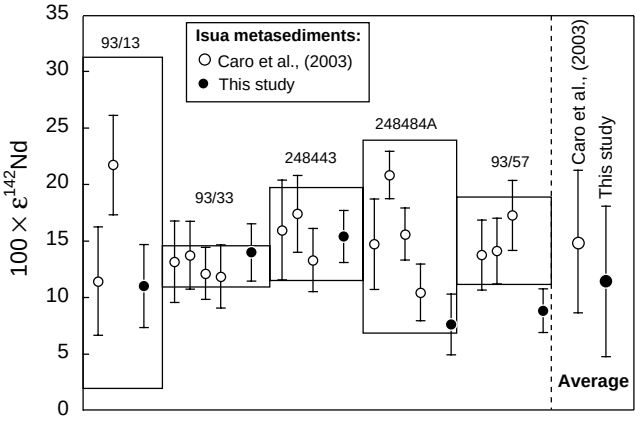

Fig. 7. $\varepsilon^{142}Nd$ results for the five metasediment samples common to Caro et al. (2003a) (white dots) and this study (black dots). Boxes represent the reproducibility (2σ) of measurements for each sample from Caro et al. (2003a). Error bars represent the internal precision of individual measurements ($2\sigma_m$).

4.2. Barberton komatiite

Four mafic rock samples from the ca. 3.5 Ga Barberton greenstone belt yield homogeneous $\varepsilon^{142}Nd$ values averaging -1.1 ± 2.4 ppm (2σ), indistinguishable from modern mantle and Nd standard Ames. This result is in agreement within errors with previous measurements by Goldstein and Galer (1992). The lack of a ^{142}Nd anomaly in Barberton suggests that ^{142}Nd anomalies in depleted mantle were probably eradicated rapidly, which, as will be shown in Section 7, implies the recycling of the earliest terrestrial protocrust within less than 1 Ga. Note that the initial $\varepsilon^{143}Nd$ signature of these rocks ($\varepsilon^{143}Nd = 1.1 \pm 0.7$) is barely resolved from the chondritic value, which is consistent, to a first order, with the absence of ^{142}Nd anomalies in Barberton samples.

4.3. Acasta gneisses

One sample from the ca. 4-Ga-old Acasta gneisses has $100 \times \varepsilon^{142}\mathrm{Nd} = 0.9 \pm 1.3$ ppm $(2\sigma_m)$, indistinguishable from the Ames standard and modern mantle signatures. This new result is in agreement with those previously obtained by McCulloch and Bennett (1993) and Jacobsen and Harper (1996). The absence of a ^{142}Nd excess in Acasta is surprising as ^{142}Nd anomalies in depleted mantle are expected to decrease as early differentiated reservoirs were progressively recycled and remixed by convection (see Section 7). The extent to which the Acasta ^{142}Nd signature is representative of a 4.0 Ga mantle reservoir is, however, extremely speculative. As emphasized in Section 2.2, contrasted age constraints were obtained on the basis of U–Pb zircons dating (<4.0 Ga, Bowring and Williams, 1999) and whole rock ^{147}Sm–^{143}Nd isochron (3371 ± 89 Ma, Moorbath et al., 1997). Similarly, the Acasta whole-rock ^{147}Sm–^{143}Nd isochron has a strongly negative initial ε^{143}Nd at 3.37 Ga ($\varepsilon^{143}\mathrm{Nd} = -5.6 \pm 0.7$, Moorbath et al., 1997), which cannot be representative of the Archaean mantle at that time. The ^{147}Sm–^{143}Nd age may hence reflect either a late major metamorphic disturbance of the 4.0-Ga-old Acasta protolith, resulting in complete resetting of the ^{147}Sm–^{143}Nd system, or alternatively, derivation of Acasta rocks at 3.37 Ga from a more ancient crustal precursor. In both cases, it is unclear whether the pristine ^{142}Nd signature could have remained unchanged during these processes. Although the ^{146}Sm–^{142}Nd chronometer could not have been reset at 3.37 Ga, thorough isotopic equilibration with metamorphic fluids carrying non-radiogenic ^{142}Nd could possibly have eradicated a pristine ^{142}Nd/^{144}Nd anomaly in Acasta. Differentiation of a 4.0-Ga-old crustal protolith at 3.37 Ga may have also modified the ^{142}Nd/^{144}Nd signature if mixing occurred with younger and non-radiogenic crustal components. Further insights into the signature of Acasta mantle source might be obtainable using ^{176}Lu–^{176}Hf systematics in 4.0-Ga-old zircons. Unfortunately, there are presently no such data available (Amelin et al., 1999, 2000) and the signature of the mantle source of Acasta precursor therefore remains speculative. Hence, it cannot be excluded at this stage that the ^{142}Nd/^{144}Nd signature measured in Acasta is indeed inherited from a 4-Ga-old undifferentiated mantle. In view of these important age uncertainties, the significance of the Acasta ^{142}Nd/^{144}Nd signature seems highly uncertain and these data will not be further considered in subsequent sections.

5. Chronological constraints from coupled ^{146}Sm–^{142}Nd and ^{147}Sm–^{143}Nd systematics

Because of the rapid decay of ^{146}Sm during the Hadean era, mantle differentiation processes are unlikely to produce detectable ^{142}Nd/^{144}Nd anomalies after 4.2 Ga. The existence of positive ^{142}Nd anomalies in 3.6–3.8 Ga Isua samples therefore constrains Sm/Nd fractionation to have taken place during the first 400 Ma of Earth's history. Further refining of this first-order ^{146}Sm chronology can be obtained by coupling long-lived ^{147}Sm–^{143}Nd and short-lived ^{146}Sm–^{142}Nd chronometers in the context of a two-stage mantle–crust model (Harper and Jacobsen, 1992). In this model, the first stage represents evolution of a primitive reservoir with chondritic ^{147}Sm/^{144}Nd and ^{142,143}Nd/^{144}Nd ratios. Mantle–crust differentiation proceeds instantaneously at time t_d and is followed by distinct evolution of differentiated reservoirs. ^{142}Nd/^{144}Nd and ^{143}Nd/^{144}Nd isotopic evolution of depleted mantle during the second stage are given by:

$$\left(\frac{^{143}\mathrm{Nd}}{^{144}\mathrm{Nd}}\right)_t^{\mathrm{dm}} = \left(\frac{^{143}\mathrm{Nd}}{^{144}\mathrm{Nd}}\right)_{t_p}^{\mathrm{chur}} + \left(\frac{^{147}\mathrm{Sm}}{^{144}\mathrm{Nd}}\right)_{t_p}^{\mathrm{chur}} \left(1 - e^{\lambda_{147} t}\right) + \left(\frac{^{147}\mathrm{Sm}}{^{144}\mathrm{Nd}}\right)_{t_p}^{\mathrm{dm}} \left(e^{\lambda_{147} t_d} - e^{\lambda_{147} t}\right), \quad (5)$$

$$\left(\frac{^{142}\mathrm{Nd}}{^{144}\mathrm{Nd}}\right)_t^{\mathrm{dm}} = \left(\frac{^{142}\mathrm{Nd}}{^{144}\mathrm{Nd}}\right)_{t_p}^{\mathrm{chur}} - \frac{\left(\frac{^{146}\mathrm{Sm}}{^{144}\mathrm{Sm}}\right)_{t_0}^{\mathrm{chur}}}{\left(\frac{^{147}\mathrm{Sm}}{^{144}\mathrm{Sm}}\right)_{t_p}^{\mathrm{chur}}} \times \left\{ \left(\frac{^{147}\mathrm{Sm}}{^{144}\mathrm{Nd}}\right)_{t_p}^{\mathrm{chur}} e^{-\lambda_{146}(t_0 - t_d)} + \left(\frac{^{147}\mathrm{Sm}}{^{144}\mathrm{Nd}}\right)_{t_p}^{\mathrm{dm}} \times \left[e^{-\lambda_{146}(t_0 - t)} - e^{-\lambda_{146}(t_0 - t_d)}\right] \right\}, \quad (6)$$

where $t_0 = 4.566$ Ga, t_d is the time of mantle–crust differentiation, t_p is present-day time, and t is time running backward from present-day to t_d. Acronyms CHUR and DM indicate Chondritic Uniform Reservoir and Depleted Mantle, respectively. $\lambda_{146} = 6.74\ \mathrm{Ga}^{-1}$ and $\lambda_{147} = 6.54 \times 10^{-3}\ \mathrm{Ga}^{-1}$ are the decay constants of ^{146}Sm and ^{147}Sm (Audi et al., 1997).

As emphasized in the previous section, the homogeneous ε^{142}Nd signature of Isua metabasalts is probably the most closely representative of the contemporaneous mantle source. However, open system behavior of the ^{147}Sm–^{143}Nd system during post-magmatic alteration and metamorphic processes (Polat et al., 2003) precludes accurate determination of their initial ε^{143}Nd signature (Blichert-Toft et al., 1999; Frei et al., 2004). In contrast, metasediments were shown to have remained a closed system on a whole-rock scale for ^{147}Sm–^{143}Nd, such that a reliable initial ε^{143}Nd value of 1.9 ± 0.6 ε-units could be obtained from a whole-rock Sm–Nd regression (Kamber et al., 1998). Hence, although ^{142}Nd systematics of these metasediments appears more complex than that of metabasalts, they represent the most appropriate samples for application of coupled ^{146,147}Sm–^{142,143}Nd chronometry.

Fig. 8 illustrates graphically how a model age of differentiation can be derived from coupled ^{146,147}Sm chronometry using Eqs. (5) and (6). By taking a value of $\varepsilon^{143}\mathrm{Nd} = 1.9 \pm 0.6$ ε-units at 3744 ± 46 Ma (Kamber et al., 1998) and constraining the corresponding $100 \times \varepsilon^{142}$Nd of depleted mantle to lie between the least radiogenic metasediment value of 7.6 ± 2.7 ppm $(2\sigma_m)$ and the most radiogenic value of 15.4 ± 2.3 ppm $(2\sigma_m)$, we obtain a model age of differentia-

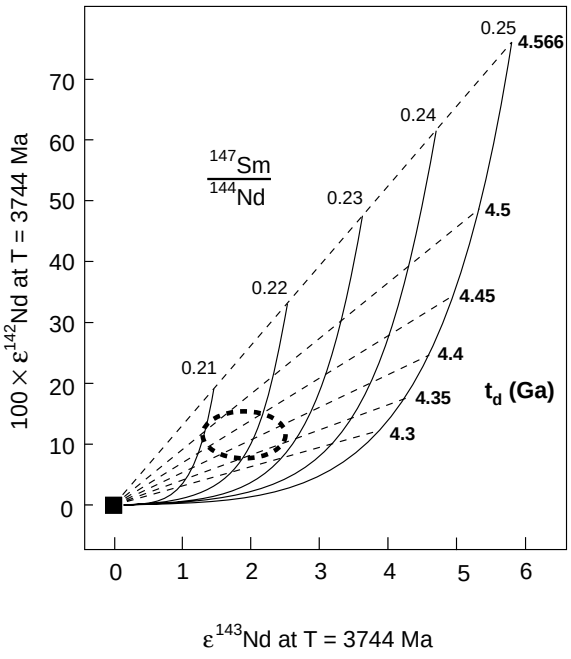

Fig. 8. Snapshot of ε^{142}Nd versus ε^{143}Nd evolution of depleted mantle at 3744 Ma. The mantle first evolves as a closed system with chondritic $^{147}Sm/^{144}Nd$ and $^{142,143}Nd/^{144}Nd$ ratios and is then depleted at t_d. Dashed lines are loci of equal differentiation ages, solid curves are loci of equal $^{147}Sm/^{144}Nd$ ratio of depleted mantle referenced to present-day time. Combined ^{142}Nd and ^{143}Nd data from Isua metasediments constrain mantle differentiation to have occurred 50–200 Ma after formation of the solar system with $^{147}Sm/^{144}Nd$ ratio of 0.21–0.23.

tion for the Earth's mantle in the range 4.35–4.50 Ga (Figs. 8 and 9). $^{147}Sm/^{144}Nd$ ratio of depleted mantle can also be estimated to ca. 0.21–0.23 (when referenced to present-day) using coupled $^{146,147}Sm$–$^{142,143}Nd$ chronometry (Fig. 8), which may suggest that early Archaean mantle was less depleted than present-day MORB source ($^{147}Sm/^{144}Nd \approx 0.23$–$0.25$; Albarède, 2001; Salters and Stracke, 2004).

Chronological results obtained from our new ^{142}Nd data indicate that differentiation of long-lived silicate reservoirs on Earth postdates the formation of the oldest meteorites by 50–200 Ma (Figs. 8 and 9). In contrast, core–mantle differentiation was probably completed after 30–50 Ma according to Hf-W chronometry (Halliday, 2004; Kleine et al., 2002; Schönberg et al., 2002; Yin et al., 2002) and U–Pb systematics (e.g., Albarède and Juteau, 1984; Allègre, 1982; Allègre et al., 1982; Galer and Goldstein, 1996). This suggests that core segregation and formation of long-lived differentiated silicate reservoirs proceeded over different timescales. In contrast, the ^{142,143}Nd model age coincides within errors with the ^{129}I–^{244}Pu–^{129}Xe age of the Earth (≈50–100 Ma) (Kunz et al., 1998; Ozima and Podosek, 1999; Staudacher and Allègre, 1982), which is interpreted as reflecting losses of atmophile elements during ongoing accretion by impact-induced volatilization. These chronological relationships suggest that large impacts have probably impeded the formation of long-lived differentiated silicate reservoirs until the final stage of terrestrial accretion (Chambers, 2001; Wetherill, 1976, 1990). As giant impacts are expected to have resulted in complete or partial melting of the mantle (Melosh, 1990), the chronological constraints derived from coupled $^{146,147}Sm$–$^{142,143}Nd$ chronometry may indicate the formation of differentiated silicate reservoirs during crystallization of a terrestrial magma ocean (e.g., Solomatov, 2000; Solomatov and Stevenson, 1993). In the next sections, we use a mantle–crust model to examine the implications of our ^{142}Nd results with respect to the formation, recycling,

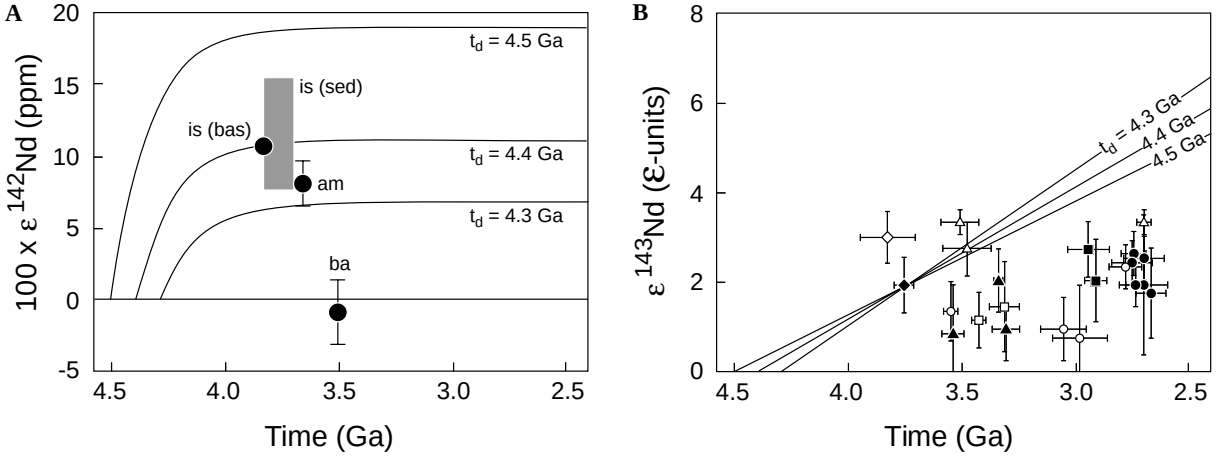

Fig. 9. (A) ε^{142}Nd and (B) ε^{143}Nd evolution of depleted mantle following instantaneous differentiation at $t_d = 4.3$, 4.4, and 4.5 Ga. $^{147}Sm/^{144}Nd$ ratio of depleted mantle is adjusted in each case to yield $\varepsilon^{143}Nd = 1.9 \pm 0.6$ ε-units at 3744 ± 46 Ma. ε^{143}Nd data are from Labrador (Canada, open diamond), Isua (Greenland, full diamond), Yilgarn (Australia, open circles), India (open squares), Kaapvaal (South Africa, full triangles), China (open triangles), Lewisian complex (Scotland, full squares), and Ontario (Canada, dark circles). All data were obtained using whole-rock ^{147}Sm–^{143}Nd isochrons (Basu et al., 1984; Carlson et al., 1983; Collerson et al., 1991; Dupré et al., 1984; Fletcher et al., 1984; Gopalan et al., 1990; Hamilton et al., 1983; Jahn et al., 1987, 1988; Moorbath et al., 1997; Morrison et al., 1985; Polat and Kerrich, 2002; Sharma et al., 1994; Shirey and Hanson, 1986; Vervoort et al., 1994; Whitehouse et al., 1996; Wilson and Carlson, 1989; Xuan et al., 1986). ba, Barberton komatiite; is (bas), Isua metabasalts; is (sed), Isua metasediments; am, Amîtsoq orthogneisses (3.65 Ga). Acasta gneisses are not represented (see discussion in text (Section 4.3)).

and composition of the Hadean crust and the timescale of mixing of heterogeneities in the early Earth's mantle.

6. A test for crustal growth models using ^{146}Sm–^{142}Nd systematics

The nature and composition of the Hadean enriched reservoir is one of the most speculative issue in the early history of the Earth. Models involving rapid growth of continental crust during the Hadean ("Big-Bang" models) were proposed by Armstrong (1968, 1981) and Jacobsen (1988a). These models imply, respectively, the formation of 100 and 50% of the present-day mass of continental crust prior to 4.0 Ga and can readily satisfy isotopic constraints from ^{147}Sm–^{143}Nd systematics. However, early formation of a basaltic crust was also shown to provide suitable $^{143}Nd/^{144}Nd$ signatures for the early Archaean depleted mantle (Chase and Patchett, 1988; Galer and Goldstein, 1991) and these models appear easier to reconcile with the lack of a widespread Hadean crustal component in Archaean sediments (Allègre and Rousseau, 1984; Miller et al., 1986; Stevenson and Patchett, 1990). Lastly, the earliest crust may have formed rapidly following accretion by melt segregation from a crystallizing magma ocean (Solomatov and Stevenson, 1993).

In this section, we test the "Big-Bang" models of continental growth (Armstrong, 1968, 1981) using a three-box model of continuous crustal growth (Jacobsen and Harper, 1996; Jacobsen and Wasserburg, 1979). We show that coupled ^{142}Nd–^{143}Nd systematics in early Archaean rocks from West Greenland are consistent with extraction of continental crust during the Hadean but would imply the formation of more than half the present-day mass of continental crust prior to 4.2 Ga.

In this model, the mantle has initially a chondritic composition and continental crust is considered to grow according to an exponentially decreasing rate:

$$\frac{dM_c}{dt} = M_c^{\infty} e^{-kt}, \tag{7}$$

where M_c represents the mass of crust, M_c^{∞} is the final mass of continental crust (2.97×10^{22} kg), and k is a constant. Equations describing the evolution of $^{142}Nd/^{144}Nd$ and $^{143}Nd/^{144}Nd$ during continuous extraction of crust are from Jacobsen and Wasserburg (1979) (model 1) and Jacobsen and Harper (1996). Note that time in Eq. (7) is running forward from the origin of solar system ($t_0 = 0$) to present-day ($t_p = 4.566$ Ga). The model involves continuous growth of depleted mantle and continental crust starting 4.5 Ga ago. The $^{147}Sm/^{144}Nd$ ratio of depleted mantle complementary to continental crust is estimated to be ≈0.23 (e.g., Jacobsen, 1988a).

The results of model calculations (Fig. 10) indicate that the $^{142}Nd/^{144}Nd$ signature of Isua metabasalts is best fitted for a value of k of 2.5 Ga^{-1}. This would imply the development of 50% of the present-day mass of continental crust prior to extinction of ^{146}Sm at 4.2 Ga and corresponds to an average growth rate of 5×10^{13} kg a^{-1} during the first 300 Ma following accretion. This estimate is approximately one order of magnitude higher than the average growth rate of continental crust during the Archaean and Proterozoic (Jacobsen, 1988a,b). If these lower values are extrapolated to the Hadean era, then they would only support the extraction of ca. 6% of present-day continental crust by 4.2 Ga, which, in turn, would generate ^{142}Nd anomalies below 7 ppm at 3.8 Ga (Fig. 10, lower curves).

It is emphasized that the growth rate derived from this study must be considered as a strict minimum. First, the development of ^{142}Nd anomalies in the mantle is strongly favored by the choice of an exponentially decreasing growth rate. If, instead, a linear or increasing growth rate is chosen, the fraction of crust produced by 4.2 Ga would have to be significantly higher to produce ^{142}Nd anomalies of ca. 10 ppm at 3.8 Ga. Second, the magnitude of ^{142}Nd anomalies in depleted mantle is strongly dependent upon

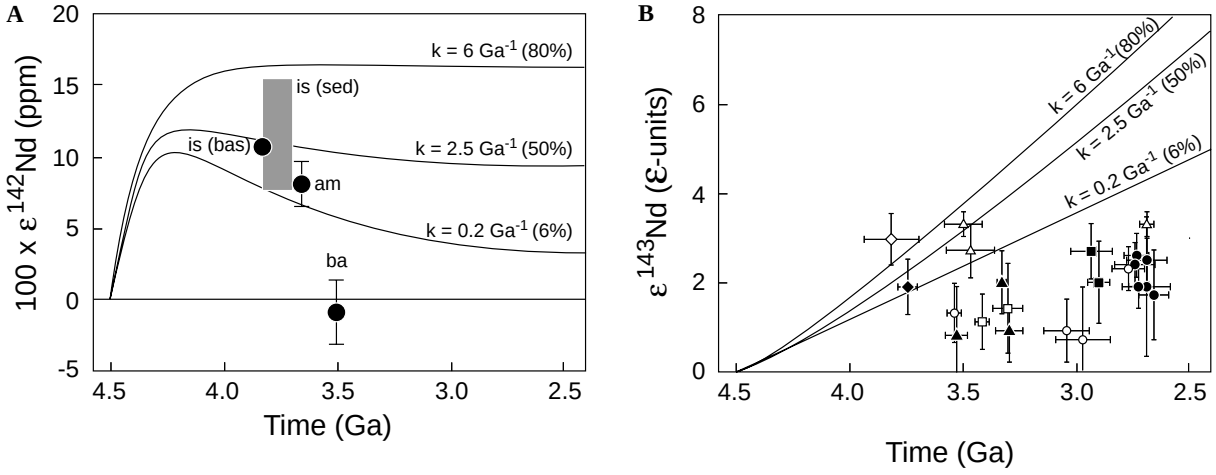

Fig. 10. (A) $\varepsilon^{142}Nd$ and (B) $\varepsilon^{143}Nd$ evolution of depleted mantle during continuous extraction of continental crust for various values of k (Eq. (7)). Values in brackets represent the mass fraction of continental crust formed at 4.2 Ga. An exponentially decreasing growth rate is used in order to maximize the response of the ^{146}Sm–^{142}Nd system to crustal growth. ^{143}Nd data compiled as in Fig. 9. ba, Barberton komatiite; is (bas), Isua metabasalts; is (sed), Isua metasediments; am, Amîtsoq orthogneisses (3.65 Ga). Acasta gneisses are not represented (see discussion in text (Section 4.3)).

the onset of crustal extraction. If crustal growth started at 4.4 Gyr, the ^{142}Nd signature of Isua metabasalts would require extraction of 80% of the present-day continental mass within less than 200 Ma and the continental crust would have reached its present-day mass prior to 4.0 Ga. This would imply an average growth rate of 1.2×10^{14} kg a^{-1}, 15–25 times higher than crustal growth rates during Archean and Proterozoic (Jacobsen, 1988b). Lastly, our calculations do not take into consideration crustal recycling. As a consequence, the average continental crust at 3.8 Ga should carry a strongly unradiogenic $^{142}Nd/^{144}Nd$ signature ($100 \times \varepsilon^{142}Nd = -25$ ppm), which is at odds with the absence of negative ^{142}Nd anomalies in metasediments and plutonic rocks from West Greenland. Considering crustal recycling would, in turn, further strengthen the need for very high growth rates in the Hadean.

These conclusions are consistent with those reached by Jacobsen and Harper (1996), who noted that their two-stage model age of mantle differentiation (calculated using $\varepsilon^{143}Nd = +4$ and $\varepsilon^{142}Nd = 33$ ppm) was almost identical to the mean crustal age calculated in the context of a continuous growth model. Although ^{142}Nd anomalies reported here are significantly lower than that considered by Jacobsen and Harper (1996), our coupled ^{142}Nd–^{143}Nd data also require the formation of a large crustal reservoir immediately following terrestrial accretion. As these high crustal growth rates bear little resemblance with those prevailing during Archaean and Proterozoic era, and appear even higher than in the most extreme "Big-Bang" model of crustal growth (Armstrong, 1968, 1981), the earliest depletion events witnessed by ^{142}Nd anomalies in early Archaean mantle may be best explained by other processes. In particular, extraction of basaltic crust by partial melting (Chase and Patchett, 1988; Galer and Goldstein, 1991) or by melt segregation during crystallization of a magma ocean (Solomatov, 2000; Solomatov and Stevenson, 1993) is both expected to proceed over short timescales (<100 Ma) and would hence be easier to reconcile with observed ^{142}Nd anomalies in Archaean mantle.

7. Modeling Nd isotopic evolution in a continuously interacting mantle–crust system

An important corollary of the chronological constraints inferred from coupled $^{146,147}Sm$–$^{142,143}Nd$ chronometry (Section 5) is that differentiated reservoirs formed near the final stage of accretion were still preserved during the early Archaean, about 700 Ma after their differentiation. This observation has important implications regarding the dynamic of the mantle–crust system during the first billion year of Earth's history. In this section, we investigate the significance of our coupled ^{142}Nd–^{143}Nd data in the context of a two-box model involving continuous exchange between crust and mantle. We propose that the magnitude of ^{142}Nd anomalies in early Archaean mantle likely reflects the lifetime of Hadean crust.

7.1. A box model for early mantle differentiation

The rates of crustal recycling in the Hadean are difficult to infer precisely because of the lack of isotopic data for the depleted mantle prior to 3.8 Ga (Jacobsen and Harper, 1996). In the case of oceanic crust formation or magma ocean crystallization, it is expected that extraction of the crustal reservoir would have proceeded rapidly (e.g., Chase and Patchett, 1988; Solomatov, 2000; Van Thienen et al., 2004). As emphasized in Section 6, very rapid differentiation is also required in the case of extraction of a continental crust. Such high crustal growth rates could not have remained constant throughout the Hadean era as they would have resulted in the production of unrealistically large amount of crust, several times the present-day mass of crust, at 4.0 Ga. This, in turn, may indicate either a sharp decrease of crustal growth rates during the first few hundred million years of Earth's history, as suggested by Jacobsen (1988a) or, alternatively, proportionate recycling rates during the Hadean. As mentioned in Section 6, the lack of negative ^{142}Nd anomalies in Archaean and modern rocks and the lack of ^{142}Nd anomaly in 3.5 Ga mantle strongly favor the latter hypothesis. In this model, we have therefore considered that a protocrust formed rapidly following terrestrial accretion. This earliest differentiation is modeled as an instantaneous process, which is similar to the two-stage model described in Section 5. We then assume that this protocrust is progressively recycled within the mantle and replaced by younger Hadean crust. For the sake of simplicity, we assume that the volume of crust and depleted mantle reservoirs remained constant over the period of interest and that the magnitude of Sm/Nd fractionation during crust formation did not vary significantly. Although these approximations represent a simplified vision of early mantle–crust evolution, they are useful in providing first-order estimates of the lifetime of earliest terrestrial protocrust. The model is schematically illustrated in Fig. 11 together with the main parameters. Note that

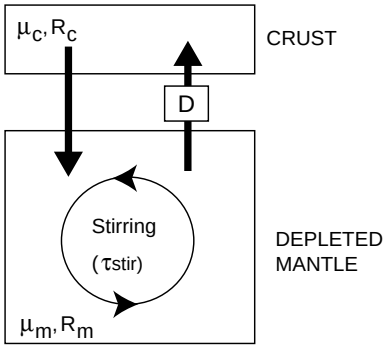

Fig. 11. Schematic illustration of the two-box mantle–crust model used in this study. Continuous extraction of material from depleted mantle is balanced by recycling. R_c and R_m stand for the residence times of Nd in mantle and crust, respectively. μ_c and μ_m represent Sm/Nd ratios of crust and mantle. τ_{stir} is the stirring time of the mantle reservoir (see Section 8) and D represents the fractionation of Sm/Nd ratio during partial melting.

mantle and crust are treated as well-mixed reservoirs. The mass transport equation reads:

$$\frac{dM_c}{dt} = \frac{dM_m}{dt} = \phi_{m\to c} - \phi_{c\to m} = 0, \quad (8)$$

where subscripts 'm' and 'c' stand for mantle and crust reservoirs, respectively, and ϕ represents the mass flux of material from crust to mantle and mantle to crust. In addition, the system is governed by the following set of mass balance equations:

$$\mu_0 = \mu_c x_c + \mu_m x_m, \quad (9)$$

$$\alpha_0 = \alpha_c x_c + \alpha_m x_m, \quad (10)$$

where subscript *0* refers to the total mantle–crust system, $\mu_{m,c} = (^{146,147}Sm/^{144}Nd)_{m,c}$, $\alpha_{m,c} = (^{142,143}Nd/^{144}Nd)_{m,c}$, and $x_{m,c}=(Nd)_{m,c}/(Nd)_0$. $(Nd)_{m,c}$ is the total amount of Nd in mantle and crust reservoir, respectively.

For each isotopic system, the evolution of mantle and crust is obtained via a three-isotope mass balance involving a stable isotope from the daughter element (^{144}Nd), the parent isotope (^{147}Sm), and the radiogenic isotope (^{142}Nd or ^{143}Nd) as described by Jacobsen and Wasserburg (1979). This yields the following set of ordinary differential equations (Albarède, 1995; Albarède and Brouxel, 1987):

$$\frac{dx_c}{dt} = \frac{x_m}{R_m} - \frac{x_c}{R_c}, \quad (11)$$

$$\frac{dx_m}{dt} = \frac{x_c}{R_c} - \frac{x_m}{R_m}, \quad (12)$$

$$\frac{d\mu_c}{dt} = \frac{x_m}{R_m x_c}(D\mu_m - \mu_c) - \lambda\mu_c, \quad (13)$$

$$\frac{d\mu_m}{dt} = \frac{1-D}{R_m}\mu_m + \frac{x_c}{R_c x_m}(\mu_c - \mu_m) - \lambda\mu_m, \quad (14)$$

$$\frac{d\alpha_c}{dt} = \frac{x_m}{R_m x_c}(\alpha_m - \alpha_c) + \lambda\mu_c, \quad (15)$$

$$\frac{d\alpha_m}{dt} = \frac{x_c}{R_c x_m}(\alpha_c - \alpha_m) + \lambda\mu_m, \quad (16)$$

where λ is the decay constant of ^{146}Sm or ^{147}Sm and t is time running forward from the time of instantaneous mantle–crust differentiation ($t_d = 0$) to present-day. D represents the Sm/Nd fractionation factor and is defined as the ratio of Sm/Nd in partial melt to that in mantle source. Initial conditions at the time of formation of the solar system (t_0) are: $^{147}Sm/^{144}Nd = 0.20264$, $^{146}Sm/^{144}Sm = 0.008$, $^{143}Nd/^{144}Nd = 0.506703$, and $^{142}Nd/^{144}Nd = 1.141545$. R_m and R_c denote the residence times of Nd in mantle and crust reservoirs, respectively, and are given by (Albarède, 2001):

$$R_c = \frac{M_c}{\phi_{c\to m}}, \quad (17)$$

$$R_m = \frac{M_m}{\beta \times \phi_{c\to m}}, \quad (18)$$

where, assuming that trace element fractionation is correctly described by an equilibrium melting process (Hofmann, 1988)

$$\beta = \frac{1}{F + D_{Nd}^{m\to c}(1-F)}, \quad (19)$$

where F is the melt fraction and $D_{Nd}^{m\to c}$ is the global partition coefficient of Nd during crustal extraction. Note that the residence time of Nd in crustal reservoir R_c is equivalent to the lifetime of the crust.

7.2. Estimating model parameters

The nature of the earliest Hadean crust is highly speculative and hence the magnitude of Sm/Nd fractionation produced by its extraction from the mantle is not known with confidence. In the particular case of extraction of continental crust, Sm/Nd fractionation can be estimated by an equilibrium melting model with $F = 1.6\%$ (Hofmann, 1988). However, the $^{143}Nd/^{144}Nd$ signature of early Archaean mantle was also shown to be consistent with extraction of basaltic protocrust formed by higher melt fraction (Chase and Patchett, 1988; Galer and Goldstein, 1991). In this model, we will initially consider extraction of a crust formed by 5% melting and we will subsequently examine the implications of using higher and lower melt fractions in the modeling. As will be shown, this parameter has only a marginal influence on the results presented here. We show that the isotopic evolution of depleted mantle is essentially controlled by the lifetime of the crustal reservoir and is only moderately affected by the magnitude of Sm/Nd fractionation occurring upon melting. Mantle–crust partition coefficients for Sm and Nd are taken from Chase and Patchett (1988) and initial conditions of the model are estimated as follows:

$$\mu_c^0 = \mu_{BSE}^0 \frac{F + D_{Nd}^{m\to c}(1-F)}{F + D_{Sm}^{m\to c}(1-F)}, \quad (20)$$

$$\mu_m^0 = \frac{D_{Sm}^{m\to c}}{D_{Nd}^{m\to c}}\mu_c^0, \quad (21)$$

$$x_c^0 = \frac{\mu_m^0 - \mu_0^0}{\mu_m^0 - \mu_c^0}, \quad (22)$$

$$x_m^0 = 1 - x_c^0. \quad (23)$$

Finally, the fractionation factor D is given by

$$D = \frac{F + D_{Nd}^{m\to c}(1-F)}{F + D_{Sm}^{m\to c}(1-F)}. \quad (24)$$

For a crust formed by 5% melting, the fraction of Nd in the crust would initially be approximately 60% of the Nd budget of the mantle–crust system. The crustal reservoir and its complementary depleted mantle would initially have a $^{147}Sm/^{144}Nd$ ratio of 0.16 and 0.25, respectively. Assuming a depleted mantle mass equivalent to the upper mantle, the

mass of crust produced would be 5×10^{22} kg, which is equivalent to a 35 km thick crust covering the whole Earth's surface. Note that this value is approximately identical to the mean crustal thickness of Hadean oceanic crust inferred from recent numerical convection models (Van Thienen et al., 2004).

7.3. Constraints on the lifetime of early Earth's crust

Eqs. (11)–(16) were solved numerically for values of R_c between 100 Ma and 4 Ga using, a fourth-order Runge–Kutta scheme. The corresponding isotopic evolutions of depleted mantle for ε^{142}Nd and ε^{143}Nd are shown in Fig. 12. The results show that extraction of crust with a lifetime of ≈800 Ma gives the best fit to the $^{142}Nd/^{144}Nd$ signature of metabasalts from West Greenland. This result is only weakly dependent upon the melt fraction considered in the calculation as estimates of R_c range between 700 Ma for $F = 1.6\%$ and 950 Ma for $F = 10\%$. We therefore estimate the lifetime of earliest crust in the range 0.7–1 Ga. According to this model, ^{142}Nd anomalies would have reached a maximum of ca. 20 ppm at 4.2–4.3 Ga, after which the average ε^{142}Nd anomaly decreased progressively. Ultimately, ^{142}Nd anomalies were erased about 1.5 Ga after the final stage of terrestrial accretion, in agreement with the absence of ^{142}Nd anomaly in modern mantle. As shown in Fig. 12, the corresponding ^{143}Nd evolution of depleted mantle between 2.7 and 4.0 Ga shows good agreement with the observed values. Note also that the evolution curve predicted by the model matches well the apparent constant signature of Archaean mantle prior to the main crustal growth stages at 2.7 Ga.

The long-term isolation of Hadean protocrust required to produce the Nd isotope signature of Archaean rocks can be interpreted as reflecting either the lifetime of continental or basaltic crust at the Earth's surface (e.g., Galer and Goldstein, 1991; Jacobsen, 1988a) or the storage of recycled basaltic crust at the core–mantle boundary (Chase and Patchett, 1988; Tolstikhin and Hofmann, 2005). If the latter is correct, the residence time of 0.7–1 Ga calculated in this model would then represent an average residence time of recycled crust at the bottom of the mantle before its re-entrainment in the convective layer. If a fraction of this recycled crust still remains stored at the core–mantle boundary, then recycled material with negative $^{142}Nd/^{144}Nd$ anomalies might still be sampled by plume volcanism. In contrast, if one accepts that the residence time reflects isolation of a crustal reservoir at the surface of the Earth, then the model would predict that remnants of the Hadean crust survived up to the middle Archaean. If this crust were analogous to modern continental crust (Armstrong, 1968, 1981; Jacobsen, 1988a,b), then a significant contribution of Hadean material would be expected in Archaean continental mass. However, the lack of a widespread >4.0-Ga-old detrital component in Archaean sediments (Allègre and Rousseau, 1984; Miller et al., 1986; Stevenson and Patchett, 1990), and the absence of crustal-derived granitoids in the most ancient Archaean terranes

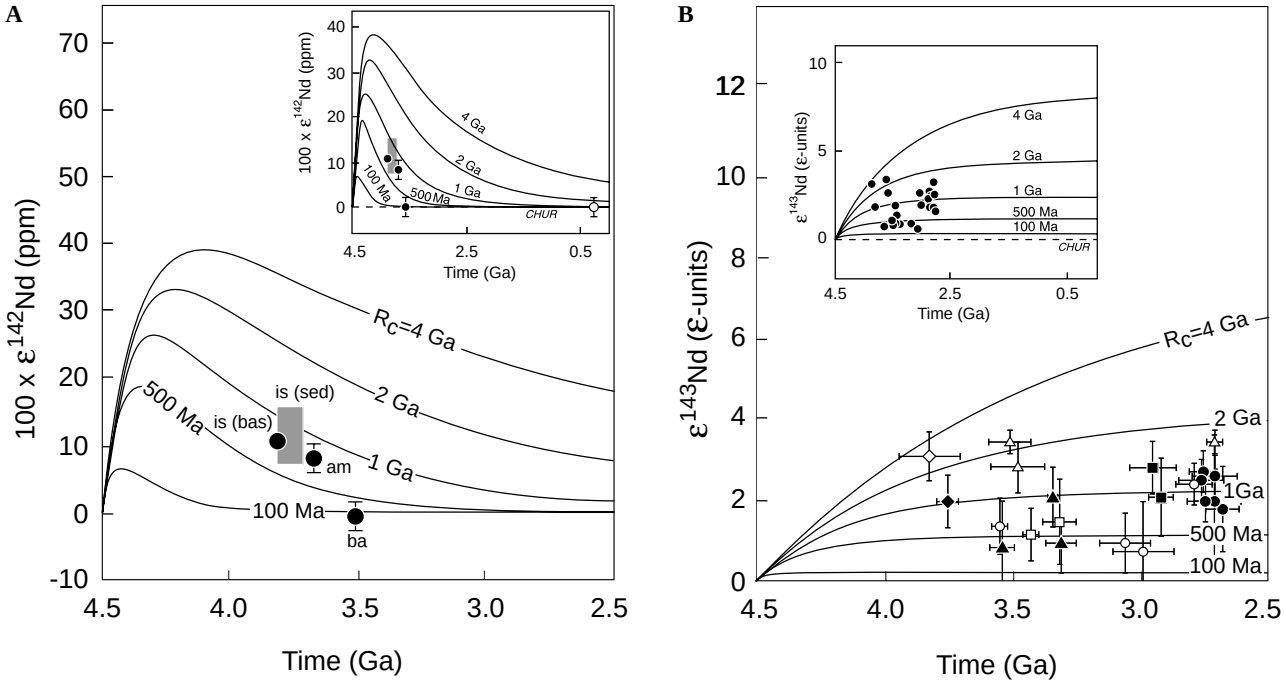

Fig. 12. (A) ε^{142}Nd and (B) ε^{143}Nd evolution of depleted mantle modeled in the context of a continuously interacting mantle–crust system for values of R_c between 100 Ma and 4 Ga. The crust is considered to form by 5% melting (see discussion in text). ε^{142}Nd data of Isua metabasalts are best fitted by a value of R_c of 800 Ma. Corresponding evolution curves of depleted mantle for ε^{143}Nd show good consistency with data from Archaean rocks. ^{143}Nd data are compiled as in Fig. 9. ba, Barberton komatiite; is (bas), Isua metabasalts; is (sed), Isua metasediments; am, Amitsoq orthogneisses (3.65 Ga). Acasta gneisses are not represented (see discussion in text (Section 4.3)).

(Kreissig and Elliott, 2005; Moorbath et al., 1972), tend to suggest that the development of sialic crust on a global scale did not occur until ca. 3.5–4.0 Ga. As suggested by Chase and Patchett (1988) and Galer and Goldstein (1991), Hadean crust may have therefore been mostly basaltic in composition.

In the context of plate tectonics, the lifetime of oceanic crust is approximately equivalent to the age of plates at subduction. Lifetime of modern oceanic crust can therefore be estimated to ca. 60 Ma (Parsons, 1982) and this timescale is expected to become shorter when extrapolated back in the past as a result of higher rates of heat production in the mantle (Bickle, 1978; Hargraves, 1986). However, as illustrated in Fig. 12, extraction of Hadean protocrust with a lifetime comparable to, or shorter than, oceanic crust would erase anomalous ^{142}Nd signature of depleted mantle prior to 4.0 Ga. In addition, the corresponding ^{143}Nd/^{144}Nd evolution of depleted mantle would only slightly depart from a chondritic value, in contrast with ^{143}Nd/^{144}Nd ratios of Archaean rocks, which typically range between +1 and +3 ε-units. This suggests that simple extrapolation of modern crustal extraction processes at spreading ridges to the Hadean era could only produce the mantle depletion recorded by ^{142,143}Nd isotopes if Hadean oceanic crust experienced long-term storage at the core–mantle boundary (Chase and Patchett, 1988).

The extent to which plate tectonics was operative in the early Earth is speculative. In particular, it has been outlined that a young and hot oceanic crust would be positively buoyant and therefore would not easily undergo subduction (e.g., Arndt, 1983; Baer, 1977; Davies, 1992). Recent numerical modeling suggests that adequate conditions for subduction of oceanic crust would not be reached prior to 4.0 Ga (Van Hunen et al., 2004). This, in turn, may have favored the preservation of a long-lived static crust during the Hadean era (e.g., Galer and Goldstein, 1991; Morgan and Phillips, 1983), in agreement with the results presented here. Interestingly, a long-lived basaltic Hadean crust is also suggested by Pb-isotope systematics of various rock types from the 3.6–3.8 Ga Greenland craton. Kamber et al. (2003) noticed that banded iron formations, detrital metasediments, and tonalitic gneisses from Isua and Amîtsoq intersect the mantle evolution curve of Kramers and Tolstikhin (1997) at significantly younger apparent ages than inferred from Pb isotope whole-rock isochron. This was interpreted by the authors as reflecting input of radiogenic Pb from a basaltic crust with ^{238}U/^{204}Pb $\approx$ 10 extracted from convective mantle at 4.1–4.3 Ga. This observation hints at the formation of basaltic protocrust in the Hadean with a lifetime of several hundred million years.

Our results therefore indicate that long-term isolation of the earliest protocrust is required by the presence of ^{142}Nd anomalies in 3.6–3.8 Ga mantle. Progressive recycling of this early crustal reservoir is then expected to have generated chemical and isotopic heterogeneities in early Earth's mantle. However, the homogeneous ^{142}Nd signature observed in modern oceanic basalts suggests that this primordial heterogeneity has now been eradicated by convective mixing. In the next section, we investigate in the framework of the two-box model illustrated in Fig. 11 the timescale of mixing of chemical and isotopic heterogeneities in the early Earth's mantle.

8. Mantle mixing and thermal state of the early Earth

In the two-box model presented in the previous section, depleted mantle is treated as a well-mixed, homogeneous reservoir. In reality, however, mixing of recycled material in the convective mantle is not instantaneous but proceeds at a rate proportional to the Lagrangian strain rate (Olson et al., 1984). Accordingly, the isotopic evolution of the depleted mantle for ^{142}Nd/^{144}Nd and ^{143}Nd/^{144}Nd of Fig. 12 only represents averages over the whole mantle reservoir and does not take into consideration isotopic heterogeneity arising from incomplete mixing of recycled material. However, ^{142}Nd/^{144}Nd and ^{143}Nd/^{144}Nd ratios of early Archean rocks exhibit significant scatter around the mean evolution curve of depleted mantle, suggesting that ^{142,143}Nd isotope signatures of early Archaean rocks represent a record of mantle heterogeneity during the first billion years of Earth's history. In this section, we present a model describing the evolution of isotopic heterogeneity of a mantle reservoir in the framework of the two-box mantle–crust system illustrated in Fig. 11. From the Nd isotope record of Archaean rocks, we estimate a characteristic timescale for mantle mixing during the first billion years of Earth's history.

8.1. Constraining isotopic heterogeneity of the early Earth's mantle using ^{146}Sm–^{142}Nd and ^{147}Sm–^{143}Nd systematics

The isotopic dispersion observed in modern oceanic basalts represents a direct record of the heterogeneity of the Earth's mantle (Allègre and Lewin, 1995; Kellogg et al., 2002). Although such record is not available for the Archaean era, the variations of isotopic signature in crustal rocks from different Archaean cratons can be used similarly to modern oceanic basalts to constrain large-scale mantle heterogeneity early in Earth history (Blichert-Toft and Albarède, 1994).

To estimate isotopic dispersion of ^{143}Nd/^{144}Nd ratio in Archean mantle, we have compiled data from Labrador (3.9 Ga), Greenland (3.6–3.8 Ga), Australia (3.4–3.7 Ga), South Africa (3.3–3.5 Ga), China (3.5 Ga), India (3.4 Ga), Scotland (2.9 Ga), and North Canada (2.7 Ga) (Ref. as in Fig. 9). To avoid spurious dispersion related to post-magmatic alteration processes, we selected only data obtained from whole-rock Sm–Nd isochrons with ages agreeing with independent chronological constraints (e.g., U–Pb zircon ages). Initial ε^{143}Nd from Acasta and Kambalda were therefore discarded (Chauvel et al., 1985; Moorbath et al., 1997). Fig. 13 shows that ε^{143}Nd of Archaean cratons range between +1 and +3 ε-units with

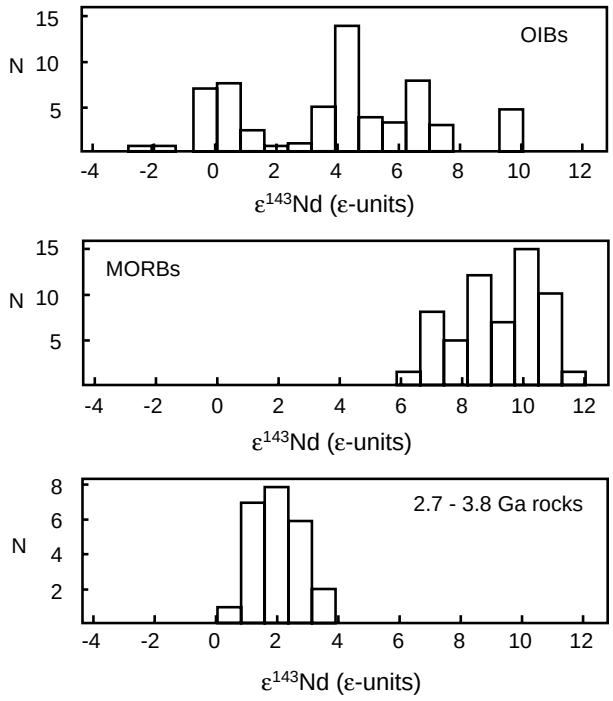

Fig. 13. ^{143}Nd isotopic dispersion observed in modern oceanic island basalts, mid-ocean ridge basalts, and Archaean rocks. Note that Archaean rocks display significantly less dispersion than modern oceanic basalts, suggesting that Archaean mantle was more homogeneous than present-day mantle. Histograms for OIBs and MORBs are from Allègre and Lewin (1995).

average $\varepsilon^{143}Nd$ of about +2 ε-units. Based on this dataset, we calculate that $^{143}Nd/^{144}Nd$ heterogeneity of 2.7–3.9 Ga Archaean mantle is about 1.5 ε-units (2σ). By comparison, isotopic dispersion in modern oceanic basalts is about 5 ε-units (2σ), whereas heterogeneity observed in modern MORBs is approximately 3 ε-units (2σ) (Allègre and Lewin, 1995) (Fig. 13). It may be noted that interlaboratory biases may also contribute to the apparent dispersion of $\varepsilon^{143}Nd$ in Archaean rocks. The above estimate of mantle heterogeneity hence probably represents an upper estimate.

Isotopic heterogeneity of early Archaean depleted mantle for $^{142}Nd/^{144}Nd$ is less well constrained since ^{142}Nd anomalies have only been reported so far from a single craton. However, a crude estimate of $^{142}Nd/^{144}Nd$ dispersion in early Archean mantle can be deduced from the magnitude of ^{142}Nd anomalies in rocks from West Greenland (Fig. 6).

8.2. Modeling isotopic heterogeneity

In the general context of a continuously interacting mantle–crust system, the dispersion of chemical ($^{146,147}Sm/^{144}Nd$) and isotopic ($^{142,143}Nd/^{144}Nd$) ratios can be described as the sum of sources and sinks of heterogeneity. In the mantle reservoir, continuous extraction of crust by partial melting and input of recycled crustal material create chemical and isotopic dispersion, whereas convective stirring tends to erase these heterogeneities. In addition, radioactive decay tends to reduce chemical heterogeneity, but increases isotopic heterogeneity. Following Allègre and Lewin (1995), chemical and isotopic heterogeneity of mantle reservoir can be related to the stirring time using the following set of ordinary differential equations:

$$\frac{\mathrm{d}\langle\mu\rangle_{\mathrm{m}}(t)}{\mathrm{d}t} = \frac{\Delta\langle\mu\rangle(t)}{R_{\mathrm{m}}} - \left\{\lambda + \frac{1}{\tau_{\mathrm{stir}}}\right\}\langle\mu\rangle_{\mathrm{m}}(t), \tag{25}$$

$$\frac{\mathrm{d}\langle\alpha\rangle_{\mathrm{m}}(t)}{\mathrm{d}t} = \lambda\langle\mu\rangle_{\mathrm{m}}(t) + \frac{\Delta\langle\alpha\rangle(t)}{R_{\mathrm{m}}} - \frac{\langle\alpha\rangle_{\mathrm{m}}(t)}{\tau_{\mathrm{stir}}}, \tag{26}$$

where $\langle\mu\rangle_{\mathrm{m}}$ and $\langle\alpha\rangle_{\mathrm{m}}$ represent standard deviation (usually noted σ) of $^{146,147}Sm/^{144}Nd$ and $^{142,143}Nd/^{144}Nd$ ratios, respectively. The stirring time τ_{stir} is the time necessary to reduce heterogeneity by a factor e in the absence of any additional input. t is time running forward from the time of mantle–crust differentiation (t_{d}) to present-day. $\Delta\langle\mu\rangle$ is defined as (Allègre and Lewin, 1995)

$$\Delta\langle\mu\rangle(t) = \langle\mu\rangle_{\mathrm{c}}(t) - \langle\mu\rangle_{\mathrm{m}}(t), \tag{27}$$

where $\langle\mu\rangle_{\mathrm{c}}$ is the chemical heterogeneity of recycled material about the mean mantle value $\overline{\mu_{\mathrm{m}}}$.

$\langle\mu\rangle_{\mathrm{c}}$ can be approximated as the sum of the intrinsic chemical heterogeneity of recycled material and the difference between mean chemical ratios of crust versus mantle reservoirs (Allègre and Lewin, 1995)

$$\langle\mu\rangle_{\mathrm{c}}(t) \approx \langle\mu\rangle_{\mathrm{c}}^{\mathrm{i}}(t) + |\overline{\mu_{\mathrm{c}}}(t) - \overline{\mu_{\mathrm{m}}}(t)|, \tag{28}$$

where $\langle\mu\rangle_{\mathrm{c}}^{\mathrm{i}}$ is the intrinsic chemical heterogeneity of crustal reservoir around its mean value $\overline{\mu_{\mathrm{c}}}$. Here, we introduce the notation $\Delta\overline{\mu}(t)$

$$\Delta\overline{\mu}(t) = |\overline{\mu_{\mathrm{c}}}(t) - \overline{\mu_{\mathrm{m}}}(t)|. \tag{29}$$

Considering that intra-crustal heterogeneity is negligible, Eq. (27) then becomes

$$\Delta\langle\mu\rangle(t) = \Delta\bar{\mu}(t) - \langle\mu\rangle_{\mathrm{m}}(t). \tag{30}$$

Likewise, a similar expression is obtained for $\Delta\langle\alpha\rangle(t)$

$$\Delta\langle\alpha\rangle(t) = \Delta\bar{\alpha}(t) - \langle\alpha\rangle_{\mathrm{m}}(t). \tag{31}$$

Eqs. (25) and (26) finally read:

$$\frac{\mathrm{d}\langle\mu\rangle_{\mathrm{m}}(t)}{\mathrm{d}t} = \frac{\Delta\bar{\mu}(t)}{R_{\mathrm{m}}} - \left\{\lambda + \frac{1}{\tau_{\mathrm{stir}}} + \frac{1}{R_{\mathrm{m}}}\right\}\langle\mu\rangle_{\mathrm{m}}(t), \tag{32}$$

$$\frac{\mathrm{d}\langle\alpha\rangle_{\mathrm{m}}(t)}{\mathrm{d}t} = \lambda\langle\mu\rangle_{\mathrm{m}}(t) + \frac{\Delta\bar{\alpha}(t)}{R_{\mathrm{m}}} - \left\{\frac{1}{\tau_{\mathrm{stir}}} + \frac{1}{R_{\mathrm{m}}}\right\}\langle\alpha\rangle_{\mathrm{m}}(t). \tag{33}$$

Allègre and Lewin (1995) showed that derivative terms in Eqs. (32) and (33) can be eliminated when chemical and isotopic heterogeneity $\langle\mu\rangle_{\mathrm{m}}$ and $\langle\alpha\rangle_{\mathrm{m}}$ reach steady state (i.e., when $t \gg \tau_{\mathrm{stir}}$). However, in the context of our model, evolution of chemical and isotopic heterogeneity is considered over timescales equivalent to the characteristic timescale of mantle mixing. The steady-state assumption is not valid and, in contrast with Allègre and Lewin (1995), the evolution of mean values ($\Delta\bar{\mu}$ and $\Delta\bar{\alpha}$) must be estimated independently.

It may be noted that the development of heterogeneity similar to that observed in Archaean mantle (Fig. 13) may not necessarily require the involvement of a recycled crustal component. Indeed, mixing of depleted and primitive mantle reservoirs would also, to a lesser extent, generate isotopic heterogeneity in the mantle. However, examination of ^{142,143}Nd data in Archaean rocks indicates that several aspects of the isotopic evolution of depleted mantle are best explained by balanced exchanges between crust and mantle (Section 7). In particular, low recycling rates would produce increasing ε^{143}Nd signature in Archaean mantle, in contrast to the relatively constant value of +2 ε-units observed prior to ca. 2.7 Ga (Fig. 10). This would also imply the preservation of ^{142}Nd anomalies in the mantle over timescales significantly longer than 1 Ga (Fig. 12), which, in turn, would be inconsistent with the absence of ^{142}Nd anomalies in Barberton and modern samples. In this model, we have considered that the development of mantle heterogeneity was primarily controlled by recycling of Hadean crust in depleted mantle. Equations describing the evolution of isotopic and chemical heterogeneity are therefore coupled with the two-box model illustrated in Fig. 11.

8.3. Mantle mixing in the early Earth

Eqs. (32) and (33) show that evolution of chemical and isotopic dispersions in the mantle reservoir depends on (i) the stirring time (τ_{stir}), (ii) the differential of mean ^{146,147}Sm/^{144}Nd and ^{142,143}Nd/^{144}Nd ratios of crust and mantle reservoirs ($\Delta\bar{\mu}$ and $\Delta\bar{\alpha}$), and (iii) the residence time of Nd in mantle reservoir (R_m). As shown in the previous section, the evolution of $\Delta\bar{\mu}$ and $\Delta\bar{\alpha}$ through time can be estimated with a mantle–crust model using Eqs. (13)–(16), respectively. The residence time of Nd in mantle reservoir is related to the crustal lifetime R_c estimated in previous section by Eqs. (17)–(19).

Eqs. (32) and (33) were solved numerically for values of τ_{stir} ranging between 100 Ma and 1 Ga, together with Eqs. (11)–(16) describing the evolution of the mean chemical and isotopic ratios of each reservoir. Results for isotopic dispersion (Fig. 14) indicate that ^{142}Nd/^{144}Nd heterogeneity reaches a maximum at 4.2–4.0 Ga, after which it decays exponentially as a result of mantle stirring. In contrast, the model ^{143}Nd/^{144}Nd heterogeneities reach an approximately steady-state value after 0.5–1 Ga, under the combined effect of mantle stirring and radioactive decay. To compare our model results with ^{143}Nd/^{144}Nd and ^{142}Nd/^{144}Nd signature of Archaean rocks, it is convenient to represent isotopic dispersion as a 2σ envelope around the mean isotopic evolution of depleted mantle. The results show that ε^{143}Nd heterogeneity of Archaean mantle yields an estimate for the stirring time of 100–250 Ma (Fig. 15), in broad agreement with ε^{142}Nd data in Archaean rocks. Higher values of τ_{stir} would generate significantly more isotopic heterogeneity than observed for ^{143}Nd/^{144}Nd and ^{142}Nd/^{144}Nd ratios. By comparison, Allègre and Lewin (1995) estimated a stirring time of 900 Ma from the slope of the correlation of oceanic basalt lavas in a ^{207}Pb/^{204}Pb versus ^{206}Pb/^{204}Pb diagram, while Kellogg et al. (2002) calculated a stirring time in the range 250–750 Ma from the observed isotopic dispersion in ^{87}Sr/^{86}Sr and ^{143}Nd/^{144}Nd of oceanic basalts. Since these estimates are based on the dispersion of isotope ratios observed in modern mantle-derived rocks, they are relevant to the recent history of the Earth. In contrast, the model presented here relies on mantle-derived rocks formed between 4.0 and 2.7 Ga. Hence, we propose that the shorter stirring time inferred from Nd isotope dispersion in early Archaean rocks reflects more efficient mixing in the hotter early Earth's mantle. Note that there is no contradiction between the long crustal lifetime of 0.7–1 Ga calculated in Section 7 and the short stirring time deduced from the dispersion of isotopic data in early Archaean rocks. Indeed, the stirring time is essentially related to the efficiency of mantle convection (Olson et al., 1984) while the lifetime of a crustal reservoir is also dependent upon the tectonic regime and the composition of the crust (see discussion in Section 7.3). Therefore, the evolution of stirring time throughout Earth's history is not expected to be directly related to that of crustal lifetime.

Theoretical models of thermal evolution predict that terrestrial mantle was hotter during the early Archaean as a result of enhanced heat production by decay of radioactive

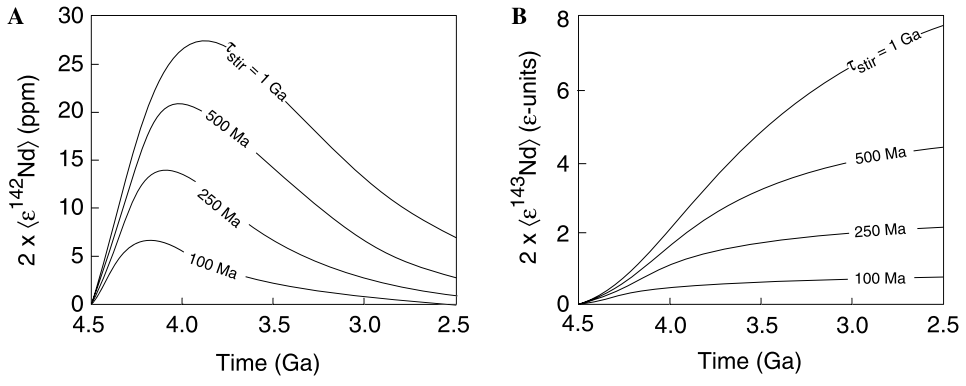

Fig. 14. Evolution of isotopic heterogeneity of depleted mantle for (A) ε^{142}Nd and (B) ε^{143}Nd calculated for various values of the stirring time τ_{stir}. A value of $R_c = 800$ Ma, (corresponding to the case illustrated in Fig. 12) is used in the calculation.

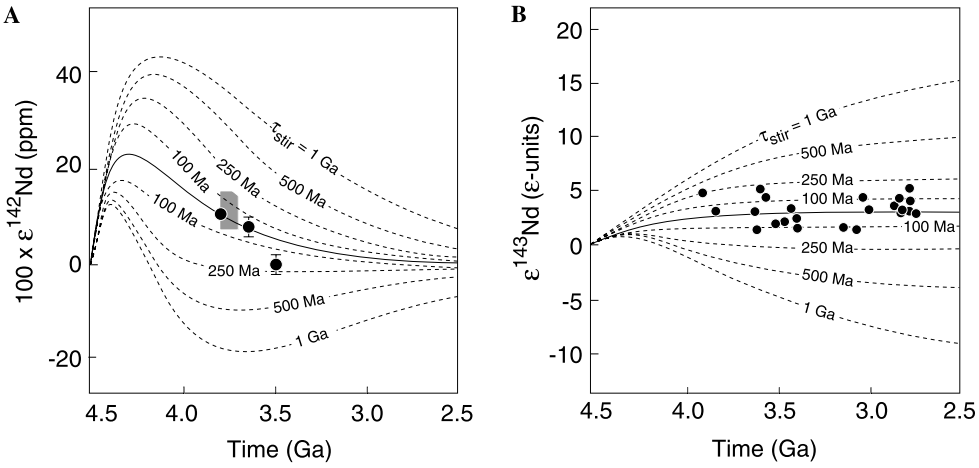

Fig. 15. (A) ε^{142}Nd and (B) ε^{143}Nd evolution of depleted mantle and corresponding isotopic heterogeneity. Solid curves represent the mean evolution of mantle reservoirs, dashed curves represent the 2σ envelope of isotopic heterogeneity for various values of the stirring time τ_{stir}. ^{143}Nd heterogeneity observed in Archaean rocks is best fitted with a value of $\tau_{stir} = 100$ Ma. This value is consistent with observed ε^{142}Nd dispersion of early Archaean rocks. Plotted data are the same as in Fig. 12. Error bars are not shown for the sake of clarity.

nuclides (e.g., Christensen, 1985; Cook and Turcotte, 1981; Schubert et al., 1980). As a hotter and less viscous mantle is bound to be correlated with higher convective velocities, the Earth's mantle is expected to have been chemically more homogeneous in the past (e.g., Blichert-Toft and Albarède, 1994). The decrease in mantle temperature since the Archaean is constrained by convection models and petrological observations to range between 50–100 °C (e.g., Campbell and Griffiths, 1992; Jarvis and Campbell, 1982) and 200–300 °C (e.g., Abbott et al., 1994; McKenzie, 1984; Nisbet and Fowler, 1983). Depending on the temperature drop since the Archaean, mantle viscosity would have been 1–3 orders of magnitudes lower than its present-day value (Christensen, 1985; Cook and Turcotte, 1981; Schubert et al., 1980), which is estimated to be 10^{21}–10^{23} Pa s (e.g., Cathles, 1975; Kaufmann and Lambeck, 2000; Peltier, 1976). This, to a first order, would be consistent with a significantly shorter stirring time in early Earth's mantle (Olson et al., 1984). The large uncertainties surrounding the thermal evolution of the early Earth preclude a confident assessment of Hadean mantle viscosity. Nevertheless, as more ^{142}Nd data in early Archaean rocks will become available, the ^{146}Sm–^{142}Nd may become a powerful tracer of mixing in Hadean mantle and could be used to further constrain the thermal evolution of the very early Earth.

9. Conclusions

We have measured with high precision ^{142}Nd^{144}Nd ratios of early Archaean rocks in order to investigate the very early history of the Earth's mantle. Our results provide new constraints regarding the chronology and nature of earliest mantle differentiation processes as well as the dynamic of the mantle–crust system during the Hadean era. The main conclusions of this study can be summarized as follows:

(1) Repeated measurements of the Ames Nd standard from August 2003 to January 2004 indicate that external precision of 2 ppm (2σ) can be achieved for ^{142}Nd/^{144}Nd ratio. This represents an improvement by a factor of 5–10 compared with previous generations of mass spectrometers. The secondary mass fractionation effect reported in Caro et al. (2003a,b) is shown to result from a magnetic field located in the source of the mass spectrometer, which could be easily eliminated. Consequently, the double normalization procedure applied to our former data is no longer necessary for accurate correction of Nd isotope measurements.

(2) We report systematic deviations of 8–15 ppm of the ^{142}Nd/^{144}Nd ratio in metasediments, metabasalts, and orthogneisses from the 3.6 to 3.8 Ga Greenland craton. These new results are consistent within errors with our initial report of a ^{142}Nd excess in Isua metasediments (Caro et al., 2003a). In contrast, Acasta gneiss and Barberton komatiite display ^{142}Nd signature indistinguishable from Ames standard and modern oceanic basalts.

(3) ^{142}Nd anomalies in rims and cores of pillowed metabasalts are homogeneous at the 2 ppm level of precision and do not seem to have been significantly modified during metamorphic processes. This observation has important implications regarding the lack of sensitivity of ^{142}Nd/^{144}Nd ratio of Archaean rocks to post-magmatic alteration.

(4) In the context of a simple two-stage model, coupled ^{147}Sm–^{143}Nd and ^{146}Sm–^{142}Nd chronometry indicates that Earth's mantle experienced large-scale differentiation 50–200 Ma after formation of the oldest meteorites. This suggests that ^{142}Nd anomalies may reflect solidification of a magma ocean soon after the final stage of terrestrial accretion.

(5) Subsequent evolution of the crust–mantle system during the first billion years of Earth's history has been investigated using a two-box model. ^{142}Nd and ^{143}Nd isotopic dispersion observed in early Archaean rocks constrain the stirring time of Earth's mantle during the first billion years to approximately 100–250 Ma. This timescale is significantly shorter than the value of 900 Ma obtained using a similar parameterization by Allègre and Lewin (1995) from modern oceanic basalts, indicating that mantle mixing was more efficient during the first billion years of Earth's history. As a consequence, the preservation of ^{142}Nd anomalies in terrestrial mantle up to 3.65–3.8 Ga requires that early differentiated reservoirs remained isolated over relatively long timescales (≈0.7–1 Ga). Inefficient crustal recycling during the Hadean era and/or long-term storage of recycled crust at the core–mantle boundary may have significantly delayed rehomogenization of early differentiated crust and mantle, and favored the long-term preservation of a mantle reservoir with positive ^{142}Nd anomalies.

Acknowledgments

The authors greatly acknowledge Samuel Henri, Geoff Davies, Richard O'Connell, Stéphane Labrosse, and Allen Nutman for helpful discussions. Informal review by Vickie Bennett was greatly appreciated. Hans Schwieters and Dietmar Tuttas are thanked for helping us maintain the Triton in optimum conditions. S.M. thanks P.W.U. Appel for much help during the field work which was supported by the Danish Natural Science Research Council, the Commission for Scientific Research in Greenland, and the Bureau of Minerals and Petroleum, Nuuk, Greenland, within the framework of the Isua Multidisciplinary Research Project. The paper benefited from reviews by Jon Patchett, Stein Jacobsen, and an anonymous reviewer and helpful comments by AE S. Galer. This work was supported by the CNRS research programs IT and PNP.

Associate editor: Stephen J.G. Galer

References

Abbott, D., Burgess, L., Longhi, J., Smith, W.H.F., 1994. An empirical thermal history of the Earth's upper mantle. *J. Geophys. Res.* **99**, 13835–13850.

Agee, C.B., Walker, D., 1989. Comments on "Constraints on element partition coefficients between $MgSiO_3$ perovskite and liquid determined by direct measurements" by T. Kato, A.E. Ringwood, and T. Irifune. *Earth Planet. Sci. Lett.* **94**, 160–161.

Albarède, F., 1995. *Introduction to Geochemical Modeling*. Cambridge University press, Cambridge.

Albarède, F., 2001. Radiogenic ingrowth in systems with multiple reservoirs: applications to the differentiation of the crust-mantle system. *Earth Planet. Sci. Lett.* **189**, 59–73.

Albarède, F., Brouxel, M., 1987. The Sm/Nd secular evolution of the continental crust and the depleted mantle. *Earth Planet. Sci. Lett.* **82**, 25–35.

Albarède, F., Juteau, M., 1984. Unscrambling the lead model ages. *Geochim. Cosmochim. Acta* **48**, 207–212.

Albarède, F., Télouk, P., Blichert-Toft, J., Boyet, M., Agranier, A., Nelson, B., 2004. Precise and accurate isotopic measurements using multiple-collector ICPMS. *Geochim. Cosmochim. Acta* **68**, 2725–2744.

Allègre, C.J., 1982. Chemical geodynamics. *Tectonophysics* **81**, 109–132.

Allègre, C.J., Dupré, B., Brévart, O., 1982. Chemical aspects of the formation of the core. *Phil. Trans. R. Soc. Lond. A* **306**, 49–59.

Allègre, C.J., Lewin, E., 1995. Isotopic systems and stirring times of the earth's mantle. *Earth Planet. Sci. Lett.* **136**, 629–646.

Allègre, C.J., Rousseau, D., 1984. The growth of the continents through geological time studied by Nd isotope analysis of shales. *Earth Planet. Sci. Lett.* **67**, 19–34.

Amelin, Y., 2004. Sm–Nd systematics of zircon. *Chem. Geol.* **211**, 375–387.

Amelin, Y., Rotenberg, E., 2004. Sm–Nd systematics of chondrites. *Earth Planet. Sci. Lett.* **223**, 267–282.

Amelin, Y., Lee, D.-C, Halliday, A.N., Pidgeon, R.T., 1999. Nature of the Earth's earliest crust from Hafnium isotopes in single detrital zircons. *Nature* **399**, 252–255.

Amelin, Y., Lee, D.-C, Halliday, A.N., 2000. Early-middle Archaean crustal evolution deduced from Lu–Hf and U–Pb isotopic studies of single zircons grains. *Geochim. Cosmochim. Acta* **64**, 4205–4225.

Appel, P.W.U., Fedo, C.M., Moorbath, S., Myers, J.S., 1998. Recognizable primary volcanic and sedimentary features in a low-strain domain of the highly deformed, oldest known (3.7–3.8 Gyr) Greenstone Belt, West Greenland. *Terra Nova* **10**, 57–62.

Armstrong, R.L., 1968. A model for the evolution of strontium and lead isotopes in a dynamic Earth. *Rev. Geophys.* **6** (2), 175–199.

Armstrong, R.L., 1981. The case for crustal recycling on a near-steady-state no-continent-growth Earth. *Phil. Trans. R. Soc. Lond. A* **301**, 443–472.

Arndt, N.T., 1983. Role of a thin, komatiite-rich oceanic crust in the Archean plate-tectonic process. *Geology* **11**, 372–375.

Audi, G., Bersillon, O., Blachot, J., Wapstra, A.H., 1997. The NUBASE evaluation of nuclear and decay properties. *Nucl. Phys.* **A624**, 1–124.

Baer, A.J., 1977. Speculations on the evolution of the lithosphere. *Precamb. Res.* **5**, 249–260.

Basu, A.R., Goodwin, A.M., Tatsumoto, M., 1984. Sm–Nd study of Archean alkalic rocks from the Superior Province of the Canadian Shield. *Earth Planet. Sci. Lett.* **70**, 40–46.

Bickle, M.J., 1978. Heat loss from the Earth: a constraint on Archaean tectonics from the relation between geothermal gradients and the rate of plate production. *Earth Planet. Sci. Lett.* **40**, 301–315.

Bizzarro, M., Baker, J.A., Haack, H., Ulbeck, D., Rosing, M.T., 2003. Early history of Earth's crust–mantle system inferred from hafnium isotopes in chondrites. *Nature* **421**, 931–933.

Blichert-Toft, J., Albarède, F., 1994. Short-lived chemical heterogeneities in the Archean mantle with implications for mantle convection. *Science* **263**, 1593–1596.

Blichert-Toft, J., Albarède, F., Rosing, M., Frei, R., Bridgwater, D., 1999. The Nd and Hf isotopic evolution of the mantle through the Archean. Results from the Isua supracrustals, West Greenland, and from the Birimian terranes of West Africa. *Geochim. Cosmochim. Acta* **63**, 3901–3914.

Bolhar, R., Kamber, B.S., Moorbath, S., Whitehouse, M.J., Collerson, K.D., 2005. Chemical characterisation of earth's most ancient clastic sediments from the Isua Greenstone Belt, southern West Greenland. *Geochim. Cosmochim. Acta* **69**, 1555–1573.

Bowring, S.A., Housh, T., 1995. The Earth's early evolution. *Science* **269**, 1535–1540.

Bowring, S.A., Williams, I.S., 1999. Priscoan (4.00–4.03 Ga) orthogneisses from northwestern Canada. *Contrib. Mineral. Petr.* **134**, 3–16.

Bowring, S.A., Williams, I.S., Compston, W., 1989. 3.96 Ga gneisses from the Slave Province, Northwest Territories, Canada. *Geology* **17**, 971–975.

Bowring, S.A., Housh, T.B., Isachsen, C.E., 1990. The Acasta gneisses: remnant of earth's early crust. In: Newsom, H.E., Jones, J.H. (Eds.), *Origin of the Earth*. Oxford University Press, New York, pp. 319–343.

Boyet, M., Carlson, R.W., 2004. New search for ^{142}Nd anomaly in kimberlites and carbonatites. *Eos Trans. AGU* **85** (47). Abstr.

Boyet, M., Blichert-Toft, J., Rosing, M.T., Storey, M., Télouk, P., Albarède, F., 2003. ^{142}Nd evidence for early Earth differentiation. *Earth Planet. Sci. Lett.* **214**, 427–442.

Brévart, O., Dupré, B., Allègre, C.J., 1986. Lead–Lead age of komatiitic lavas and limitations on the structure and evolution of precambrian mantle. *Earth Planet. Sci. Lett.* **77**, 293–302.

Campbell, I.H., Griffiths, R.W., 1992. The changing nature of mantle hotspots through time: implications for the chemical evolution of the mantle. *J. Geol.* **92**, 497–523.

Carlson, R.W., Hunter, D.R., Barker, F., 1983. Sm–Nd age and isotopic systematics of the bimodal suite, ancient gneiss complex, Swaziland. *Nature* **305**, 701–704.

Caro, G., Bourdon, B., Birck, J.-L., Moorbath, S., 2002. $^{142}Nd/^{144}Nd$ precise determination in early Archaean rocks. *Geochim. Cosmochim. Acta* **66**, A120, abstr.

Caro, G., Bourdon, B., Birck, J.-L., Moorbath, S., 2003a. ^{146}Sm–^{142}Nd evidence from Isua metamorphosed sediments for early differentiation of the Earth's mantle. *Nature* **423**, 428–432.

Caro, G., Bourdon, B., Birck, J.-L., Moorbath, S., 2003b. Corrigendum to "^{146}Sm–^{142}Nd evidence from Isua metamorphosed sediments for early differentiation of the Earth's mantle". *Nature* **424**, 974.

Cathles, L.M., 1975. *The Viscosity of the Earth's mantle*. Princeton University Press, Princeton, NJ.

Chambers, J.E., 2001. Making more terrestrial planets. *Icarus* **152**, 205–224.

Chase, C.G., Patchett, P.J., 1988. Stored mafic/ultramafic crust and early Archean mantle depletion. *Earth Planet. Sci. Lett.* **91**, 66–72.

Chauvel, C., Dupré, B., Jenner, G.A., 1985. The Sm–Nd age of Kambalda volcanics is 500 Ma too old! Earth Planet. *Sci. Lett.* **74**, 315–324.

Christensen, U.R., 1985. Thermal evolution models for the Earth. *J. Geophys. Res.* **90**, 2995–3007.

Collerson, K.D., Campbell, L.M., Weaver, B.L., Palacz, Z.A., 1991. Evidence for extreme mantle fractionation in early Archaean ultramafic rocks from northern Labrador. *Nature* **349**, 209–214.

Compston, W., Pidgeon, R.T., 1986. Jack Hills, evidence of more very old detrital zircons in Western Australia. *Nature* **321**, 525–534.

Cook, F.A., Turcotte, D.L., 1981. Parameterized convection and the thermal evolution of the Earth. *Tectonophysics* **75**, 1–17.

Crowley, J.L., 2003. U-Pb geochronology of 3810-3630 Ma granitoid rocks south of the Isua Greenstone Belt, southern West Greenland. *Precamb. Res.* **126**, 235–257.

Crowley, J.L., Myers, J.S., Dunning, G.R., 2002. Timing and nature of multiple 3700–3600 Ma tectonic events in intrusive rocks north of the Isua greenstone belt, Southern West Greenland. *Bull. Geol. Soc. Am.* **114**, 1311–1325.

Davies, G.F., 1992. On the emergence of plate tectonics. *Geology* **20**, 963–966.

Dupré, B., Chauvel, C., Arndt, N.T., 1984. Pb and Nd isotopic study of two Archean komatiitic flows from Alexo, Ontario. *Geochim. Cosmochim. Acta* **48**, 1965–1972.

Fletcher, I.R., Rosman, K.J.R., Williams, I.R., Hickman, A.H., Baxter, J.L., 1984. Sm–Nd geochronology of greenstone belts in the Yilgarn block, Western Australia. *Precamb. Res.* **26**, 333–361.

Frei, R., Polat, A., Meibom, A., 2004. The Hadean upper mantle conundrum: evidence for source depletion and enrichment from Sm–Nd, Re–Os and Pb isotopic compositions in 3.71 Gy boninite-like metabasalts from the Isua Supracrustal Belt, Greenland. *Geochim. Cosmochim. Acta* **68**, 1645–1660.

Friend, C.R.L., Bennett, V.C., Nutman, A.P., 2002. Abyssal peridotites >3800 Ma from southern West Greenland: field relationships, petrography, geochronology, whole-rock and mineral chemistry of dunite and harzburgite inclusions in the Itsaq gneiss complex. *Contrib. Mineral. Petr.* **143**, 71–92.

Froude, D.O., Ireland, T.R., Kinny, P.D., Williams, I.S., Compston, W., Williams, I.R., Myers, J.S., 1983. Ion microprobe identification of 4100–4200 Myr old terrestrial zircons. *Nature* **304**, 616–618.

Galer, S.J.G., Abouchami, W., 2004. Mass bias correction laws suitable for MC-ICP-MS measurement. *Geochim. Cosmochim. Acta* **68**, A542. Abstr.

Galer, S.J.G., Goldstein, S.L., 1991. Early mantle differentiation and its thermal consequences. *Geochim. Cosmochim. Acta* **55**, 227–239.

Galer, S.J.G., Goldstein, S.L., 1996. Influence of accretion on lead in the Earth. In: Basu, A.R., Hart, S.R. (Eds.), *Earth Processes: Reading The Isotopic Code*, vol. 95. AGU Geophysical Monograph, pp. 75–98.

Goldstein, S.L., Galer, S.J.G., 1992. On the trail of early mantle differentiation: $^{142}Nd/^{144}Nd$ ratios of early Archean rocks. *Eos Trans. AGU* **73** (S323). Abstr.

Gopalan, K., MacDougall, J.D., Roy, A.B., Murali, A.V., 1990. Sm–Nd evidence for 3.3 Ga old rocks in Rajasthan, northwestern India. *Precamb. Res.* **48**, 287–297.

Gruau, G., Rosing, M., Bridgewater, D., Gill, R.C.O., 1996. Resetting of Sm–Nd systematics during metamorphism of >3.7-Ga rocks: implications for isotopic models of early Earth differentiation. *Chem Geol.* **133**, 225–240.

Halliday, A.N., 2004. Mixing, volatile loss and compositional change during impact-driven accretion of the Earth. *Nature* **427**, 505–509.

Hamilton, P.J., O'Nions, R.K., Evensen, N.M., 1979. Sm–Nd dating basic and ultrabasic volcanics. *Earth Planet. Sci. Lett.* **32**, 293–302.

Hamilton, P.J., O'Nions, R.K., Bridgwater, D., Nutman, A.P., 1983. Sm–Nd studies of Archaean metasediments and metavolcanics from West Greenland and their implications for the Earth's early history. *Earth Planet. Sci. Lett.* **62**, 263–272.

Hargraves, R.B., 1986. Faster spreading or greater ridge length in the Archean? *Geology* **14**, 750–752.

Harper, C.L., Jacobsen, S.B., 1992. Evidence from coupled ^{147}Sm–^{143}Nd and ^{146}Sm–^{142}Nd systematics for very early (4.5 Gyr) differentiation of the Earth's mantle. *Nature* **360**, 728–732.

Hayashi, M., Komiya, T., Nakamura, Y., Maruyama, S., 2000. Archaean regional metamorphism of the Isua supracrustal belt, southern west Greenland: Implications for a driving force for Archaean plate tectonics. *Internat. Geol. Rev.* **42**, 1055–1115.

Hofmann, A.W., 1988. Chemical differentiation of the Earth: the relationship between mantle, continental crust, and oceanic crust. *Earth Planet. Sci. Lett.* **90**, 297–314.

Jacobsen, S.B., 1988a. Isotopic and chemical constraints on mantle–crust evolution. *Geochim. Cosmochim. Acta* **52**, 1341–1350.

Jacobsen, S.B., 1988b. Isotopic constraints on crustal growth and recycling. *Earth Planet. Sci. Lett.* **90**, 315–329.

Jacobsen, S.B., Dymek, R.F., 1988. Nd and Sr isotope systematics of clastic metasediments from Isua, West Greenland: Identification of pre-3.8 Ga differentiated crustal components. *J. Geophys. Res.* **39**, 338–354.

Jacobsen, S.B., Harper, C.L., 1996. Accretion and early differentiation history of the Earth based on extinct radionuclides. In: Basu, A., Hart, S. (Eds.), *Earth Processes: Reading The Isotopic Code*, vol. 95. AGU Geophysical monograph, pp. 47–74.

Jacobsen, S.B., Wasserburg, G.J., 1979. The mean age of mantle and crustal reservoirs. *J. Geophys. Res.* **84**, 7411–7424.

Jacobsen, S.B., Wasserburg, G.J., 1984. Sm–Nd evolution of chondrites and achondrites, II. *Earth Planet. Sci. Lett.* **67**, 137–150.

Jahn, B.M., Auvray, B., Cornichet, J., Bai, Y.L., Shen, Q.H., Liu, D.Y., 1987. 3.5 Ga old amphibolites from eastern Hebei province, China: field occurrence, petrography, Sm–Nd isochron age and REE geochemistry. *Precamb. Res.* **34**, 311–346.

Jahn, B.M., Auvray, B., Shen, Q.H., Liu, D.Y., Zhang, Z.Q., Dong, Y.J., Ye, X.J., Zhang, Q.Z., Cornichet, J., Mace, J., 1988. Archean crustal evolution in China: the Taishan complex, and evidence for juvenile crustal addition from long-term depleted mantle. *Precamb. Res.* **38**, 381–403.

Jarvis, G.T., Campbell, I.H., 1982. Archean komatiites and geotherms: solutions to an apparent contradiction. *Geophys. Res. Lett.* **10**, 1133–1136.

Kamber, B.S., Moorbath, S., Whitehouse, M.J., 1998. Extreme Nd isotope heterogeneity in the early Archaean—fact or fiction? Case

histories from northern Canada and West Greenland-Reply. *Chem. Geol.* **148**, 219–224.

Kamber, B.S., Moorbath, S., Whitehouse, M.J., 2001. The oldest rocks on Earth: time constraints and geological controversies. In: Lewis, S.J., Knell, C.L.E. (Eds.), *The Age of the Earth: From 4004 BC to AD 2002*. Spec. Pub. Geol. Soc., Lond., vol. 190, pp. 177–203.

Kamber, B.S., Collerson, K.D., Moorbath, S., Whitehouse, M.J., 2003. Inheritance of early Archaean Pb-isotope variability from long-lived Hadean protocrust. *Contrib. Mineral. Petr.* **145**, 25–46.

Kato, T., Ringwood, A.E., Irifune, T., 1988. Experimental determination of element partitioning between silicate perovskites, garnets and liquids: constraints on early differentiation of the mantle. *Earth Planet. Sci. Lett.* **89**, 123–145.

Kato, T., Ringwood, A.E., Irifune, T., 1989a. Constraints on element partition coefficients between $MgSiO_3$ perovskite and liquid determined by direct measurements. *Earth Planet. Sci. Lett.* **90**, 65–68.

Kato, T., Ringwood, A.E., Irifune, T., 1989b. Constraints on element partition coefficients between $MgSiO_3$ perovskite and liquid determined by direct measurements—reply to C.B. *Agee D. Walker. Earth Planet. Sci. Lett.* **94**, 162–164.

Kaufmann, G., Lambeck, K., 2000. Mantle dynamics, postglacial rebound and the radial viscosity profile. *Phys. Earth Planet. Inter.* **121**, 301–324.

Kellogg, J.B., Jacobsen, S.B., O'Connell, J.R., 2002. Modeling the distribution of isotopic ratios in geochemical reservoirs. *Earth Planet. Sci. Lett.* **204**, 183–202.

Kleine, T., Münker, C., Mezger, K., Palme, H., 2002. Rapid accretion and early core formation of asteroids and terrestrial planets from Hf-W chronometry. *Nature* **418**, 952–955.

Kramers, J.D., Tolstikhin, I.N., 1997. Two terrestrial lead isotope paradoxes, forward transport modeling, core formation and the history of the continental crust. *Chem. Geol.* **139**, 75–110.

Kreissig, K., Elliott, T., 2005. Ca isotope fingerprints of early crust–mantle evolution. *Geochim. Cosmochim. Acta* **69**, 165–176.

Kunz, J., Staudacher, T., Allègre, C.J., 1998. Plutonium-fission xenon found in Earth's mantle. *Science* **280**, 877–880.

Lugmair, G.W., Galer, S.J.G., 1992. Age and isotopic relationships between among the angrite Lewis Cliff 86010 and Angra Dos Reis. *Geochim. Cosmochim. Acta* **56**, 1673–1694.

Lugmair, G.W., Marti, K,, 1977. Sm–Nd–Pu timepieces in the Angra Dos Reis meteorite. *Earth Planet. Sci. Lett.* **35**, 273–284.

Lugmair, G.W., Scheinin, N.B., Marti, K., 1983. Samarium-146 in the early solar system: evidence from Neodymium in the Allende meteorite. *Science* **222**, 1015–1018.

McCulloch, M.T., Bennett, V.C., 1993. Evolution of the early Earth: constraints from ^{143}Nd–^{142}Nd isotopic systematics. *Lithos* **30**, 237–255.

McKenzie, D.P., 1984. The generation and compaction of partially molten rocks. *J. Petrol.* **25**, 713–765.

Melosh, H.J., 1990. Giant impacts and the thermal state of the early Earth. In: Newson, H.E., Jones, J.H. (Eds.), *Origin of the Earth*. Oxford Univ Press, New York, pp. 69–84.

Miller, R.G., O'Nions, R.K., Hamilton, P.J., Welin, E., 1986. Crustal residence ages of clastic sediments, orogeny and continental evolution. *Chem. Geol.* **57**, 87–99.

Moorbath, S., O'Nions, R.K., Pankhurst, R.J., Gale, N.H., McGregor, V.R., 1972. Further rubidium–strontium age determinations on the very early Precambrian rocks of the Godthaab district, West Greenland. *Nat. Phys. Sci.* **240**, 78–82.

Moorbath, S., Whitehouse, M.J., Kamber, B.S., 1997. Extreme Nd-isotope heterogeneity in the early Archaean- fact or fiction? Case histories from northern Canada and west Greenland. *Chem. Geol.* **135**, 213–231.

Morgan, P., Phillips, R.J., 1983. Hot spot heat transfer: its application to Venus and implications to Venus and Earth. *J. Geophys. Res.* **88**, 131–299.

Morrison, D.A., Davis, D.W., Wooden, J.L., Bogard, D.D., Maczuga, D.E., Phinney, W.C., Ashwal, L.D., 1985. Age of the Mulcahy Lake intrusion, northwest Ontario, and implications for the evolution of greenstone-granite terrains. *Earth Planet. Sci. Lett.* **73**, 306–316.

Nisbet, E.G., Fowler, C.M.R., 1983. Model for Archean plate tectonics. *Geology* **11**, 376–379.

Nutman, A.P., Bennett, V.C., Friend, C.R.L., Rosing, M.T., 1997. ≈3710 and ⩾3790 Ma volcanic sequences in the Isua (Greenland) greenstone belt; structural and Nd isotope implications. *Chem. Geol.* **141**, 271–287.

Nutman, A.P., Bennett, V.C., Friend, C.R.L., Norman, M.D., 1999. Meta-igneous (non-gneissic) tonalities and quartz–diorite from an extensive ca. 3800 Ma terrain south of the Isua supracrustal belt, southern West Greenland: constraints on early crust formation. *Contrib. Mineral. Petr.* **137**, 364–388.

Nyquist, L.E., Bogard, D.D., Wiesmann, H., Bansal, B., Shih, C.Y., Morris, R.M., 1990. Age of a eucrite clast from the Bholghati howardite. *Geochim. Cosmochim. Acta* **54**, 2195–2206.

Nyquist, L.E., Bansal, B., Wiesmann, H., Shih, C.Y., 1994. Neodymium, strontium and chromium isotopic studies of the LEW86010 and Angra dos Reis meteorites and the chronology of the angrite parent body. *Meteoritics* **29** (1994), 872–885.

Ohtani, E., 1988. Chemical stratification of the mantle formed by melting in the early stage of the terrestrial magma ocean. *Tectonophysics* **154**, 201–210.

Olson, P., Yuen, D.A., Balsiger, D., 1984. Mixing of passive heterogeneities by mantle convection. *J. Geophys. Res.* **89** (B1), 425–436.

Ozima, M., Podosek, F.A., 1999. Formation age of the Earth from $^{129}I/^{127}I$ and $^{244}Pu/^{238}U$ systematics and the missing Xe. *J. Geophys. Res.* **104** (B11), 25493–25499.

Parsons, B., 1982. Causes and consequences of the relation between area and age of the ocean floor. *J. Geophys. Res.* **87**, 289–302.

Patchett, P.J., Vervoort, J.D., Söderlund, U., Salters, V.J.M., 2004. Lu–Hf and Sm–Nd isotopic systematics in chondrites and their constraints on the Lu–Hf properties of the Earth. *Earth Planet. Sci. Lett.* **222**, 29–41.

Peltier, W.R., 1976. Glacial isostatic adjustment, II, The inverse problem. *Geophys. J. R. Astron. Soc.* **46**, 669–705.

Polat, A., Kerrich, R., 2002. Nd-isotope systematics of 2.7 Ga adakites, magnesian andesites, and arc basalts, Superior province: evidence for shallow crustal recycling at Archean zones. *Earth Planet. Sci. Lett.* **202**, 345–360.

Polat, A., Hofmann, A.W., Münker, C., Regelous, M., Appel, P.W.U., 2003. Contrasting geochemical patterns in the 3.7–3.8 Ga pillow basalt cores and rims, Isua greenstone belt, Southwest Greenland: implications for postmagmatic alteration processes. *Geochim. Cosmochim. Acta* **67**, 447–457.

Prinzhofer, D.A., Papanastassiou, D.A., Wasserburg, G.J., 1989. The presence of ^{146}Sm in the early solar system and implications for its nucleosynthesis. *Astrophys. J.* **344** (2), L81–L84.

Prinzhofer, D.A., Papanastassiou, D.A., Wasserburg, G.J., 1992. Samarium–neodymium evolution of meteorites. *Geochim. Cosmochim. Acta* **56**, 797–815.

Regelous, M., Collerson, K.D., 1996. ^{147}Sm–^{143}Nd, ^{146}Sm–^{142}Nd systematics of early Archaean rocks and implications for crust–mantle evolution. *Geochim. Cosmochim. Acta* **60** (18), 3513–3520.

Rehkamper, M., Gartner, M., Galer, S.J.G., Goldstein, S.L., 1996. Separation of Ce from other rare-earth elements with application to Sm–Nd and La–Ce chronometry. *Chem. Geol.* **129**, 201–208.

Rollinson, H., 2002. The metamorphic history of the Isua greenstone belt, West Greenland. In: Fowler, C.M.R., Ebinger, C.J., Hawkesworth, C.J., (Eds.), *The Early Earth: Physical, Chemical and Biological Development*, Spec. Pub. Geol. Soc. Lond., vol. 199, pp. 329–350.

Russell, W.A., Papanastassiou, D.A., Tombrello, T.A., 1978. Ca isotope fractionation in the Earth and other solar system materials. *Geochim. Cosmochim. Acta* **42**, 1075–1090.

Salters, V.J.M., Stracke, A., 2004. Composition of the depleted mantle. *Geochem. Geophys. Geosyst.* **5** (5).

Scherer, E., Münker, C., Metzger, K., 2001. Calibrating the Lu–Hf clock. *Science* **293**, 683–686.

Schönberg, R., Kamber, B.S., Collerson, K.D., Eugster, O., 2002. New W-isotope evidence for rapid terrestrial accretion and early core formation. *Geochim. Cosmochim. Acta* **66**, 3151–3160.

Schubert, G., Stevenson, D.J., Cassen, P., 1980. Whole planet cooling and the radiogenic heat source contents of the Earth and Moon. *J. Geophys. Res.* **85** (B5), 2531–2538.

Sharma, M., Chen, C., 2004. Neodymium isotope fractionation in the mass spectrometer and the issue of ^{142}Nd anomalies in early Archean rocks. *Precamb. Res.* **135**, 315–329.

Sharma, M., Basu, A.R., Ray, S.L., 1994. Sm–Nd isotopic and geochemical study of the Archean Tonalite–Amphibolite association from the eastern Indian Craton. *Contrib. Mineral. Petr.* **117**, 45–55.

Sharma, M., Papanastassiou, D.A., Wasserburg, G.J., Dymek, R.F., 1996. The issue of the terrestrial record of ^{146}Sm. *Geochim. Cosmochim. Acta* **60** (11), 2037–2047.

Shirey, S.B., Hanson, G.N., 1986. Mantle heterogeneity and crustal recycling in Archean granite-greenstone belts: evidence from Nd isotopes and trace elements in Rainy Lake area Superior Ontario, Canada. *Geochim. Cosmochim. Acta* **50**, 2631–2651.

Smith, A.D., Ludden, J.N., 1989. Nd isotopic evolution of the Precambrian mantle. *Earth Planet. Sci. Lett.* **93**, 14–22.

Söderlund, U., Patchett, J.P., Vervoort, J.D., Isachsen, C.E., 2004. The ^{176}Lu decay constant determined by Lu–Hf and U–Pb isotope systematics of Precambrian mafic intrusions. *Earth Planet. Sci. Lett.* **219**, 311–324.

Solomatov, V.S., 2000. Fluid dynamics of a terrestrial magma ocean. In: Canup, R.M., Righter, K. (Eds.), *Origin of the Earth and Moon*. The University of Arizona Press, pp. 323–338.

Solomatov, V.S., Stevenson, D.J., 1993. Non-fractional crystallization of a terrestrial magma ocean. *J. Geophys. Res.* **98** (E3), 5391–5406.

Staudacher, T., Allègre, C.J., 1982. Terrestrial xenology. *Earth Planet. Sci. Lett.* **60**, 389–406.

Stevenson, R.K., Patchett, P.J., 1990. Implications for the evolution of continental crust from Hf isotope systematics of Archean detrital zircons. *Geochim. Cosmochim. Acta* **54**, 1683–1697.

Tolstikhin, I., Hofmann, A.W., 2005. Early crust on top of the Earth's core. *Phys. Earth Planet. Int.* **148**, 109–130.

Van Hunen, J., Van den Berg, A.P., Vlaar, N., 2004. Various mechanisms to induce present-day shallow flat subduction and implications for the younger Earth: a numerical parameter study. *Phys. Earth Planet. Int.* **146**, 179–194.

Van Thienen, P., Van den Berg, A.P., Vlaar, N., 2004. Production and recycling of oceanic crust in the early Earth. *Tectonophysics* **386**, 41–65.

Vervoort, J.D., White, W.M., Thorpe, R.I., 1994. Nd and Pb isotope ratios of the Abitibi greenstone belt: new evidence for very early differentiation of the Earth. *Earth Planet. Sci. Lett.* **128**, 215–229.

Vervoort, J.D., Patchett, P.J., Gehrels, G.E., Nutman, A.P., 1996. Constraints on early Earth differentiation from hafnium and neodymium isotopes. *Nature* **379**, 624–627.

Vervoort, J.D., Patchett, P.J., Blichert-Toft, J., Albarède, F., 1999. Relationships between Lu–Hf and Sm–Nd isotopic systems in the global sedimentary. *Earth Planet. Sci. Lett.* **168**, 79–99.

Wetherill, G.W., 1976. The role of large bodies in the formation of the earth and moon. *Proc. Lunar. Sci. Conf.*, 3245–3257.

Wetherill, G.W., 1990. Formation of the Earth. *Annu. Rev. Earth Planet. Sci.* **18**, 205–256.

Whitehouse, M.J., Fowler, M.B., Friend, C.R.L., 1996. Conflicting mineral and whole-rock isochron ages from the Late-Archaean Lewisian Complex of northwestern Scotland: implications for geochronology in polymetamorphic high-grade terrains. *Geochim. Cosmochim. Acta* **60** (16), 3085–3102.

Whitehouse, M.J., Nägler, T.F., Moorbath, S., Kramers, J.D., Kamber, B.S., Frei, R., 2001. Priscoan (4.0–4.03 Ga) orthogneisses from northwestern Canada—by Samuel Bowring and Ian S. Williams: discussion. *Contrib. Mineral. Petr.* **141**, 248–250.

Wilde, S.A., Valley, J.W., Peck, W.H., Graham, C.M., 2001. Evidence from detrital zircons for the existence of continental crust and oceans on the Earth 4.4 Gyr ago. *Nature* **409**, 175–178.

Wilson, A.H., Carlson, R.W., 1989. A Sm–Nd and Pb isotope study of Archaean greenstone belts in the southern Kaapvaal Craton, South Africa. *Earth Planet. Sci. Lett.* **96**, 89–105.

Xuan, H., Ziwei, B., DePaolo, D.J., 1986. Sm–Nd isotope study of early Archean rocks, Qianan, Hebei Provice, China. *Geochim. Cosmochim. Acta* **50**, 625–631.

Yin, Q., Jacobsen, S.B., Yamashita, K., Blichert-Toft, J., Télouk, P., Albarède, F., 2002. A short timescale for terrestrial planet formation for Hf-W chronometry of meteorites. *Nature* **418**, 949–952.